sustainability

MDPI

Article

Design of Decentralized Hybrid Microgrid Integrating Multiple Renewable Energy Sources with Power Quality Improvement

Jayachandran Jayaram [1], Malathi Srinivasan [1,*], Natarajan Prabaharan [1,*] and Tomonobu Senjyu [2,*]

[1] School of Electrical & Electronics Engineering, SASTRA Deemed University, Thanjavur 613 401, India; jj_chandru@eee.sastra.edu
[2] Department of Electrical and Electronics Engineering, University of the Ryukyus, Okinawa 903-0213, Japan
* Correspondence: jj_mals@eee.sastra.edu (M.S.); prabaharan.nataraj@gmail.com (N.P.); b985542@tec.u-ryukyu.ac.jp (T.S.); Tel.: +91-9600441614 (M.S.); +91-9750785975 (N.P.)

Abstract: Due to the energy crisis and exhaustion in the amount of fossil fuels left, there is an urge to increase the penetration of renewables in the grid. This paper deals with the design and control of a hybrid microgrid (HMG) in the presence of variable renewable energy sources. The DC sub-grid consists of a permanent magnet synchronous generator (PMSG) wind turbine, solar PV array with a perturb-and-observe (P&O) MPPT algorithm, boost converter, and battery energy storage system (BESS) with DC loads. The AC sub-grid consists of a PMSG wind turbine and a fuel cell with an inverter circuit synchronized to the grid to meet its load demand. A bidirectional interlinking converter (IC) connects the AC sub-grid and DC sub-grid, which facilitates power exchange between them. The decentralized control of converters allows all the renewables to operate in coordination independently without communication between them. The proposed control algorithm of the IC enables it to act as an active power filter in addition to the power exchange operation. The active power filtering feature of the IC helps to retain the power quality of the microgrid as per IEEE 519 standards by providing reactive power support and reducing the harmonic levels to less than 5%. The HMG with the proposed algorithm can operate in both grid-connected and islanded modes. While operating in grid-connected mode, power exchange between DC and AC sub-grids takes place and all the load demands are met. If it is in islanded mode, a diesel generator supports the AC sub-grid to meet the critical load demands and the BESS supports the DC microgrid. The proposed model is designed and simulated using MATLAB-SIMULINK and its results are analyzed. The efficacy of the proposed control is highlighted by comparing it with the existing controls and testing the HMG for load variations.

Keywords: decentralized control; hybrid microgrid; renewable energy; power quality; grid-connected; islanded; BESS; diesel generator

Citation: Jayaram, J.; Srinivasan, M.; Prabaharan, N.; Senjyu, T. Design of Decentralized Hybrid Microgrid Integrating Multiple Renewable Energy Sources with Power Quality Improvement. *Sustainability* **2022**, *14*, 7777. https://doi.org/10.3390/su14137777

Academic Editors: José Luis Domínguez-García and George Kyriakarakos

Received: 24 February 2022
Accepted: 21 June 2022
Published: 25 June 2022

Publisher's Note: MDPI stays neutral with regard to jurisdictional claims in published maps and institutional affiliations.

Copyright: © 2022 by the authors. Licensee MDPI, Basel, Switzerland. This article is an open access article distributed under the terms and conditions of the Creative Commons Attribution (CC BY) license (https://creativecommons.org/licenses/by/4.0/).

1. Introduction

In the world of an increasing energy crisis, to provide community resiliency, reliability, and stability; lower the cost of energy; and promote clean energy for a safe environment, it is essential to find a limitless source of energy. The exhaustive utilization of fossil fuels has led to global warming and many environmental issues [1,2]. Thus, research is carried on for the effective utilization of renewable resources for generating clean and environmentally friendly energy. In addition, many remote locations have intermittent supply from the grid. Yet many of those areas are abundant in renewable energy sources (RES) like wind, solar, biomass, and hydro [3]. Thus, it is better to integrate renewable sources as distributed generators (DG) in those places to reduce dependency on the grid bypassing the transmission systems. The recent advancement in power electronics has

resulted in various types and scales of DC and AC loads connected to the power system [4]. All these scenarios encouraged the research on microgrids (MG), for interconnection to the grid and to meet the local energy demands [5]. As the grid is an intermittent source, it is important for a microgrid to seamlessly switch between islanded mode and grid-connected mode [6,7]. Proper controllers help the DG units to operate efficiently in both islanded and grid-connected modes. When integrating various DG units in a system, all the DG units must operate synchronously to maintain the stability of the system.

Various control algorithms are available for the coherent operation of DG units. They are broadly classified as centralized and decentralized. In a centralized control scheme, all the DG units in a system are controlled by a microgrid centralized controller (MGCC) [8]. The MGCC acts as a secondary controller that commands the individual primary controller of each DG. In this method, a communication link should be established between the MGCC and each controller. This method of control suffers from single-point failure issues and does not support plug-and-play technology. In a decentralized control scheme, all the DG units in the system operate independently without a secondary master controller. In the decentralized control method peer-to-peer interaction takes place and controllers operate effectively with local measurements themselves. This mode of the controller does not suffer from a single-point-of-failure issue and also supports plug-and-play technology [9]. In DC MG the voltage of the DC bus is the key indicator, and the controllers of DC MG DG units are designed to maintain the DC bus voltage at a reference point [10]. Similarly, in AC MG, the controllers are designed to operate in synchronization with the voltage and frequency reference signals [11–13].

As the conventional power system adopts AC due to its transmission and distribution advantages, implementing AC microgrids with AC DG units is very easy. However, many DG units, such as solar, fuel-cell, and energy storage devices, are DC in nature. Moreover, increasing DC loads led to the development of the DC microgrid. Since both AC and DC MGs have their advantages, a hybrid microgrid (HMG) combines the advantages of both [14]. The HMG constitutes three main elements: (i) DCMG, (ii) ACMG, and (iii) an interlinking converter (IC) [15]. Interconnecting AC and DC MG through a power electronic converter results in an HMG. In an HMG, a bidirectional AC-DC IC interconnects DC and AC sub-grids [12,16]. This IC supports power exchange between the AC and DC sub-grid, allowing us to integrate various types of DG units and loads with an energy storage facility. Different structures and control strategies of ICs are developed by researchers to improve the performance and power rating [15,17]. Since renewables are uncertain, they are combined with other conventional energy sources and/or energy storage systems. Generally, conventional diesel generators are used in AC sub-grids as backup during the islanded condition and low renewable generation. The voltage and frequency of the microgrid in the standalone mode can be maintained within the prescribed safe zone limit at the lowest cost by adopting a suitable voltage frequency management technique [18]. In DC, sub-grid battery energy storage systems (BESS) are installed to store the power during excess generation and utilize it later [19]. Loads of various types, such as linear, non-linear, balanced, and unbalanced, are connected to the system [20].

The recent advancements in power electronics resulted in the increased usage of converters in the MG system. Thus, the microgrid suffers from serious power-quality issues, for instance, low power factor, harmonics, voltage unbalance (sag–swell), etc. [21]. According to the IEEE-519 standards [22], the total harmonic distortion (THD) should be sustained at less than 5% and the voltage unbalance factor within 2. Custom power devices like active power filters (APFs) [23], dynamic voltage restorers, unified power flow controllers, STATCOMs [24], and series compensators play a crucial task in maintaining the power quality of the system [25]. An appropriate control algorithm for PE converters will reduce the harmonics injection, but additional compensation devices are required for mitigating harmonics due to non-linear loads [26]. APF is a widely used custom power device in the distribution system for mitigating harmonics. Various topologies and control

strategies are available for this device, but this additional device increases the cost of the overall system [27,28]. New concepts suggest that instead of installing additional power-conditioning equipment, a modified control algorithm of inverter-based DG units allows it to provide power-quality services in addition to its fundamental power transfer. One such concept in a hybrid microgrid system is virtual APF. By modifying the control algorithm of IC between the AC and DC sub-grid, it can act as a shunt APF along with its power-exchange operation [10,29]. The IC performs its basic operation of fundamental power exchange between DC and AC sub-grids, along with that it also virtually acts as an APF by providing compensation for harmonics and maintaining the system at the unity power factor by providing reactive power support.

There is an increased interest in the usage of renewable energy sources, particularly solar and wind, as they render electricity free of pollution. There are several research studies that analyze the problems related to the integration of wind and solar into the grid. Economic analysis and the impact of the integration of renewable energy sources on the existing and future smart power system for subtropical climates can be studied through the software Hybrid Optimization for Electric Renewable (HOMER) [30]. The integration of RES into the HMG involves several power electronic converters in the system. Because of this, the power quality of the grid is degraded. The power quality of the microgrid can be Improved by installing optimized STATCOM and energy-storage elements [31]. The interfacing of the solar photovoltaic array in the AC microgrid also introduces power-quality issues in the grid. With the design of a suitable control strategy for the interfacing PV inverter, the power quality of the grid can be improved under non-linear load conditions [32]. The partially shaded solar photovoltaic cells have multiple peaks in their power-to-voltage characteristics. Thus, an improved optimization technique is much needed to extract the global peak instead of the local peak. To capture the global peak at enhanced explorations, the optimization algorithm requires a greater number of search agents at the initial stage and a smaller number of search agents at the final stage. Most of the conventional optimization algorithms do not fulfill the above requirements. A musical chair algorithm is proposed in [33] for the MPPT of PV systems where the convergence time, failure rate, and steady-state oscillations are lower compared to other conventional optimization techniques.

In this paper, a solar PV with an MPPT, a PMSG wind turbine, and a BESS constitute the DC sub-grid, and the integration of a PMSG wind turbine, fuel cell, and diesel generator establishes the AC sub-grid. Decentralized control is proposed for the integration and efficient coordination of various DG units installed in the system. An interlinking converter connected between the DC and AC microgrids supports the exchange of power among the sub-grids. With the proposed control algorithm, the IC acts as virtual APF to mitigate the power-quality issues and offer reactive power support for AC loads. The control technique also monitors the seamless switching between grid-connected and islanded mode with an uninterrupted power supply during the standalone mode. The efficacy of the proposed control is highlighted by comparing it with the existing controls in Table 1. The main contributions of this paper are summarized as:

Table 1. Performance comparison of control techniques.

	Control Strategies					
Conditions	**Proposed**	**Ref. [34]**	**Ref. [35]**	**Ref. [36]**	**Ref. [37]**	**Ref. [38]**
Support of DC voltage	yes	No	yes	yes	No	yes
Support of AC voltage	yes	yes	yes	yes	yes	No
Frequency deviation	yes	No	No	No	No	No
Continuous operation of voltage sources	No	yes	yes	yes	yes	yes

Implementation to parallel interlinking converter	yes	No	No	yes	yes	yes
Seamless operation between grids	yes	No	No	No	No	No
Power-quality Improvement	yes	No	yes	No	No	No

- Designing a control technique for an interlinking converter for efficient power-sharing among the AC and DC microgrid and power-quality improvement. The proposed control effectively coordinates the power exchange between the AC and DC hybrid microgrid.
- Integration and efficient utilization of renewable energy sources by the superior operation friendliness of the AC and DC microgrids.
- The proposed control supports the bidirectional power flow between DC and AC microgrids without much deviation in the frequency and a seamless transition between grid-connected and islanded mode with minimal dependence on additional sources.

The microgrid model with the above-stated features is designed and simulated using the MATLAB/SIMULINK environment, and the results are analyzed. This paper has the following sections. In Section 1, the introduction to the topic and the literature survey are discussed. In Section 2, the configuration of the microgrid and its design are explained. In Section 3, the control scheme of the various DGs used is elaborated on. In Section 4, the performance of the system under various load conditions is analyzed based on the simulation results, and Section 5 briefs the conclusion and future work.

2. Microgrid Configuration

The schematic diagram of the proposed HMG model is shown in Figure 1. The DC sub-grid consists of a solar PV with converter, a PMSG wind turbine with converter, a BESS with converter, and DC loads that are connected to a prevailing DC bus. The AC sub-grid consists of a fuel cell with a converter, a PMSG wind turbine with converter, AC loads, and a diesel generator, which are connected to the point of common coupling (PCC) of a three-phase AC bus. The AC sub-grid is also connected to the three-phase utility power grid through a static transfer switch (STS). Both the DC and AC sub-grids are connected through an IC. The DC bus of the DC sub-grid and the DC link of the IC are connected, and the AC side of the IC is connected to the AC bus PCC through a coupling inductor. A three-phase ripple filter is connected to the PCC for filtering current and voltage ripple.

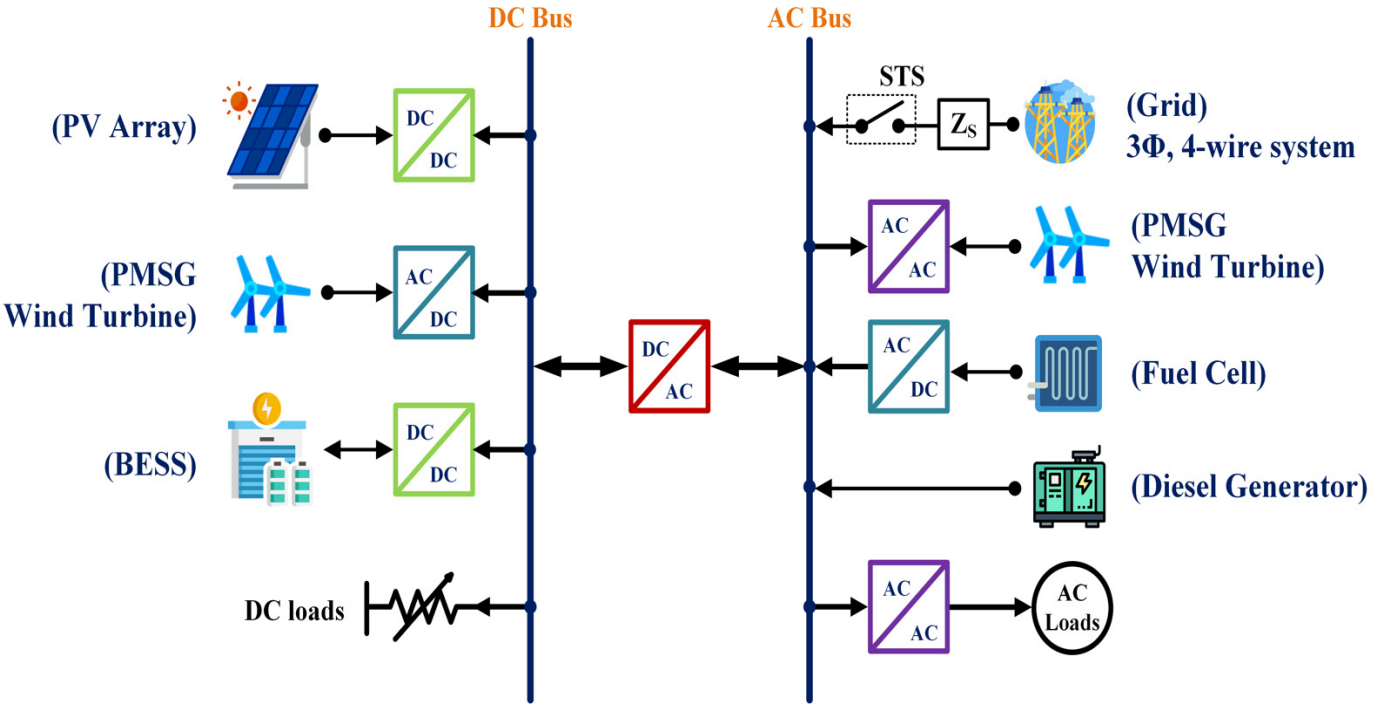

Figure 1. Schematic diagram of the hybrid microgrid.

2.1. Load

On the DC side, a variable load that varies between 10 kW and 25 kW at 700 V is connected to the common DC bus. Three single-phase non-linear loads varying between 74 kW +12 kVAr and 50 kW + 2.5 kVAr at 415 V, 50 Hz, are connected at the PCC of the AC sub-grid.

A 10 kW load on the DC side and 50 kW + 2.5 kVAr on the AC side are considered critical loads. The DC sub-grid reference voltage is set to 700 V and the AC sub-grid reference frequency and voltage are set to 50 Hz and 415 V, respectively.

2.2. PV Array Design

The PV array is designed for a rated power of 7 kW. The technical specifications of the PV module are given in Table 2. Based on the technical specifications, the number of strings and the number of modules are calculated [19].

Table 2. Technical specifications of the solar PV array.

Solar PV Array	
Model	**SunPower SPR—305WHT**
Number of cells—N_c	96
Open-circuit voltage—V_{oc}	64.2 V
Short-circuit current—I_{sc}	5.96 A
Voltage at maximum power point—V_{MP}	54.7 V
Current at maximum power point—I_{MP}	5.58 A
No. of series modules per string—NS	6
No. of parallel strings—NP	4
Maximum power extractable—Po	7 kW

$$NS = \frac{V_{dc}}{V_{oc}} = \frac{350}{64.2} = 5.45\sim6 \quad (1)$$

$$NP = \frac{P_{mp}/V_{dc}}{I_{mp}} = \frac{7000/350}{5.58} = 3.58\sim4 \quad (2)$$

where V_{oc}, I_{mp}, and P_{mp} represent the open-circuit voltage, maximum current, and maximum power of the PV module, respectively. Thus, six modules are connected in a series to form a string. Four strings are connected in parallel to obtain a power of 7 kW with a maximum voltage of 328.2 V (54.7 × 6 = 328.2).

2.3. Boost Converter Design

To extract maximum power from the PV array, an MPPT based boost converter is incorporated. A perturb-and-observe (P&O) algorithm-based boost converter is utilized to obtain the maximum power and reference voltage. The explanation for P&O is given in Section 3.1. The inductance of the boost converter is designed based on the current ripple, output DC voltage, and switching frequency [19]. Generally, 10–20% of the current is considered a ripple.

$$L_{boost}^{MPPT} = \frac{(V_{out} - V_{in})(V_{in}/V_{out})}{\Delta I_{PV} \times f} \quad (3)$$

$$L_{boost}^{MPPT} = \frac{(700 - 328.2)(328.2/700)}{4.46 \times 10000} = 3.9\ mH$$

where V_{in} represents the PV output voltage at maximum power condition; "f" represents the switching frequency of the boost converter, which is considered 10 kHz; and ΔI_{PV} represents the ripple current.

2.4. PMSG Wind Turbine

The power from wind is harnessed by converting it into torque. The kinetic energy of wind drives the blades of the wind turbine, which produces torque. This torque is used to drive the rotor shaft of the generator to produce electric power. Wind turbines use various types of generators. PMSG is the most commonly used generator. In the PMSG machine, the rotor is made up of a permanent magnet that excites the field. The stator produces three-phase AC, which is converted to DC by a diode bridge rectifier. The DC is converted back to AC and synchronized to the grid by utilizing a grid-side inverter. The mechanical power extractable from the wind is given by [39]:

$$P_m = 0.5\rho A C_p(\lambda, \beta) V_w^3 \quad (4)$$

where P_m is the mechanical power extractable from the wind, ρ is the air density, A is the rotor-swept area, V_w is the speed of the wind, and $C_p(\lambda, \beta)$ is the coefficient of power, a function of λ, β (tip-speed ratio, pitch angle). The wind turbine is designed for 12 kW at a nominal wind speed of 12 m/s.

2.5. Fuel Cell

A fuel cell is an electrochemical cell that converts chemical energy into electrical energy. It utilizes H_2 and O_2 as fuel. The reaction of hydrogen and oxygen between the anode and cathode produces electric power along with heat and water. The fuel-cell output voltage is given by [40]:

$$V_{FC} = E_{fc} - \eta_{act} - \eta_{ohm} - \eta_{con} \quad (5)$$

where V_{FC} is the output voltage of the fuel cell, E_{fc} is the internal voltage of the fuel cell, η_{act} is the fuel cell voltage drop due to activation, η_{ohm} is the voltage drop due to ohmic polarization, and η_{con} is a voltage drop due to concentration polarization. The power produced by the fuel cell is given by:

$$P_{FC} = N_0 V_{FC} I_{FC} \quad (6)$$

Here, P_{FC} is the power produced by a stack of fuel cells, N_0 is the number of cells in the stack, and I_{FC} is the stack current. A fuel cell of 30 kW at 350 V is used in this work.

2.6. Inverter

To integrate the DC output of the wind turbine and fuel cell, a grid-side inverter is used. The DC link voltage of the inverter is given by [19]:

$$V_{DC} = \frac{2\sqrt{2}\, V_{LL}}{\sqrt{3}m} = \frac{2\sqrt{2}\ \times 415}{\sqrt{3} \times 1} = 678\sim700\ V \quad (7)$$

where V_{LL} is the RMS line voltage and "m" is the modulation index.

$$C_{DC} = \frac{P_{DC}/V_{DC}}{2\omega V_{DC-Ripple}} \quad (8)$$

where C_{DC} is the DC link capacitor. For 20% of the voltage ripple, the DC link capacitance for the fuel cell and wind turbine generator is considered 5000 uF and 2000 uF, respectively.

2.7. Buck–Boost Converter

The terminal voltage of the battery is less than the DC bus voltage; thus, a buck–boost converter is used for the step-up and step-down of the voltages. In addition, for proper charging and discharging of the battery, a suitable controller is to be embedded with it. During charging of the battery, the converter is used to buck the DC bus voltage to the battery terminal voltage. For the discharging operation, the converter boosts the terminal voltage of the battery to match the DC bus voltage. The charging and discharging operations are based on the DC bus voltage level and SoC of the battery. The inductance of the buck–boost converter is designed based on the current ripple, output DC voltage, and switching frequency. Generally, 10–20% of the current is considered a ripple. For buck mode, the inductor value is selected based on Equation (9), and for boost mode, its value is calculated as per Equation (10). The largest of these inductance values is selected for the design.

$$L_{buck} > \frac{(V_{in} - V_{out})(V_{out})}{\Delta I_{PV} \times f \times V_{in\,max I_{out}}} \quad (9)$$

$$L_{boost} > \frac{(V_{out} - V_{in})(V_{in\,min})}{\Delta I_{PV} \times f \times I_{out} \times V_{out}^2} \quad (10)$$

The inductor value is set as 3 mH.

2.8. BESS

The microgrid is designed to store the excess power generation and serve a DC critical load of 10 kW for up to 6 h without any generating source [19]:

$$Ah = \frac{(P_g - P_l)t}{V_b} = \frac{(17{,}000 - 10{,}000) \times 6}{350} = 120 \quad (11)$$

where P_g is the maximum generation from DC DG units, P_l is the critical load, and V_b is the battery terminal voltage. A buck–boost charge controller is used for charging and discharging the battery, which is connected to a 700 V DC bus.

2.9. Diesel Generator

A diesel generator of 50 kVA at 415 V, 50 Hz, is designed for serving critical AC loads during the islanded condition. During the islanded condition, the diesel generator acts as the reference signal for other AC DG units.

2.10. Interlinking Converter

An IC is connected for integration and power transfer between DC and AC sub-grids. The IC's kVA rating is given by:

$$S = 3\,V_{ph} \times I_{ph} \times 1.25\ \times 10^{-3} \quad (12)$$

From Equations (7) and (8), the DC link voltage is 700 V and the capacitance is 15,000 uF. The IC is designed with a power rating of 95 kVA.

2.11. Utility Grid

A balanced three-phase four-wire utility grid of 415 V, 50 Hz, is connected to the AC sub-grid at PCC through an STS. The utility grid is modeled as a three-phase programmable voltage source with a series RL branch. The three--phase programmable voltage source generates a three-phase sinusoidal voltage with time-varying parameters. The series RL branch is connected in series with the source to account for source impedance. The values of R and L for source impedance are chosen as 1 Ω and 6 mH, respectively.

During the grid-connected mode of operation, the grid frequency, grid voltage, and phase angle are used as reference signals for AC DG units. AC DG units operate in synchronization with the grid to maintain system stability.

3. Control Algorithm

Multiple control schemes are used in the proposed microgrid. All the DG units utilize the decentralized controllers, which are discussed in the subsequent subsections.

3.1. Solar PV Control

Maximum power from the PV array can be extracted by incorporating the perturb-and-observe (P&O)-based MPPT algorithm, which is shown in Figure 2. This MPPT method is simple and efficient. In this method, the boost converter duty cycle is continuously varied by the MPPT controller for extracting the maximum power. The duty cycle is perturbed and a change in P_{PV}, and V_{PV} is observed as per the flowchart given in Figure 2. Figure 3 shows the control logic of the P&O MPPT-based boost converter. Based on the observed changes, the duty cycle is increased or decreased. The duty cycle is passed to a PWM generator, which generates the switching pulses for the boost converter. This process is repeated to achieve maximum output power.

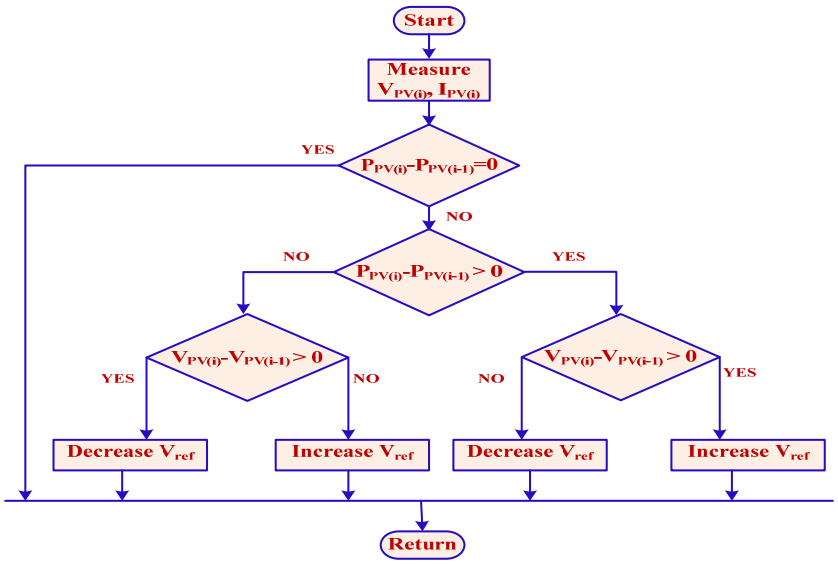

Figure 2. MPPT perturb-and-observe algorithm.

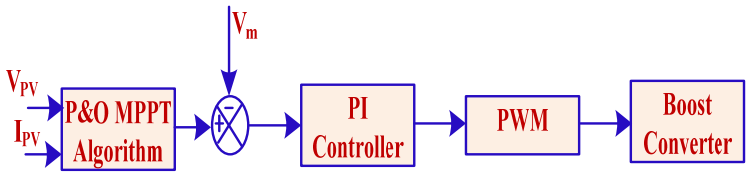

Figure 3. MPPT controller.

3.2. Inverter Control

Two separate inverters are used for integrating the wind turbine generator and a fuel cell into the AC sub-grid. Since real power injection is the prime objective of these two DG units, the inverter outputs are synchronized with the reference signal and operated in a current-controlled mode. During grid-connected mode, the frequency and voltage of the grid are used as reference signals. For stable output, the DC link of the inverter should be stabilized. So, the DC-link voltage of the inverter and reference voltage is compared, and the error signal is passed to a PI controller. The PI controller's output corresponds to power loss in the DC-link capacitor to maintain its voltage stability. The difference between the generated power and power loss across the DC link gives the required amount of power to be injected into the system. The reference signal is the grid voltage and grid frequency for grid-connected mode and the diesel-generator voltage and its frequency for islanded mode. The three-phase reference voltage is passed to a PLL block to obtain the angle Θ. Then, the voltage signal is transformed from the abc plane to the dq0 plane using Park's transformation. The reference *d*-axis current signal is obtained using the equation below:

$$i_d = \frac{2}{3}\frac{P_g V_d + Q_g V_q}{V_d^2 + V_q^2} \tag{13}$$

Since the active power is injected, the reference q-axis current signal is 0. The reference current signal is transferred back to the abc plane from the dq0 plane with angle Θ using the inverse Park's transformation. The generated reference current signal and measured inverter output current signal is sent to a hysteresis current controller to obtain the gate pulses for the inverter, as shown in Figure 4. The hysteresis controller confines the current ripples and maintains a sinusoidal inverter output current.

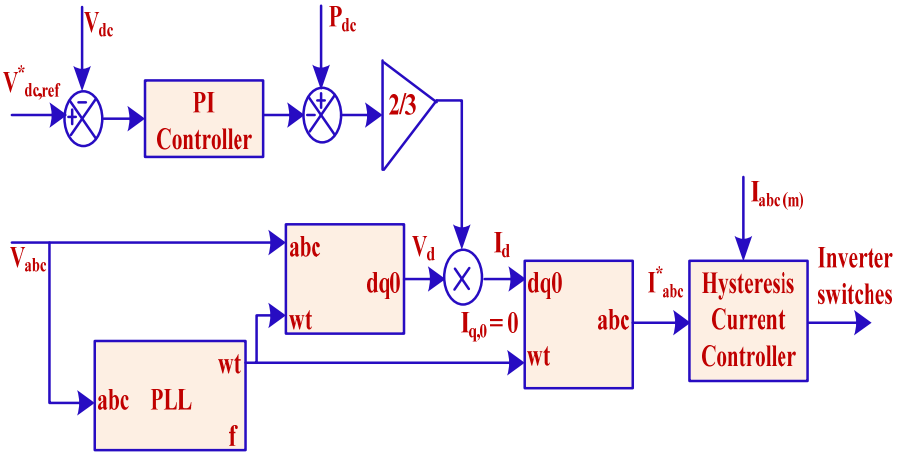

Figure 4. Inverter control logic.

3.3. BESS Control

A buck–boost converter is used for battery management. The terminal voltage of the battery is 350 V, whereas the DC bus voltage is 700 V. Hence, the voltage should be bucked from 700 V to 350 V to charge the battery, which is done by using a buck converter. During discharge, the voltage should be boosted from 350 V to 700 V. The discharging and charging of the battery are decided by the voltage of the DC bus. When the DC bus voltage is 700 V or above, the buck converter is switched and the battery charges; else, the boost converter is switched on and the battery discharges.

3.4. IC Control

In this work, the IC is designed for power exchange purposes as well as active filtering. Thus, an instantaneous reactive power theory (IRPT)-based control algorithm that is suitable for both IC and APF is implemented. In this theory, the instantaneous reactive power is calculated based on the terminal voltage and load currents of three phases. Using Clarke's transformation, the three-phase current and voltages are transformed to the α-β plane. Before the transformation, those signals are passed through a first-order Butterworth filter to remove ripples [20,41].

Clarke's transformation is carried out as follows:

$$\begin{pmatrix} V_\alpha \\ V_\beta \end{pmatrix} = \sqrt{\frac{2}{3}} \begin{pmatrix} 1 & -\frac{1}{2} & -\frac{1}{2} \\ 0 & \frac{\sqrt{3}}{2} & -\frac{\sqrt{3}}{2} \end{pmatrix} \begin{pmatrix} V_a \\ V_b \\ V_c \end{pmatrix} \tag{14}$$

Since the source is a balanced three-phase four-wire system, the zero-sequence component V_o is eliminated in Equation (14).

$$\begin{pmatrix} I_\alpha \\ I_\beta \end{pmatrix} = \sqrt{\frac{2}{3}} \begin{pmatrix} 1 & -\frac{1}{2} & -\frac{1}{2} \\ 0 & \frac{\sqrt{3}}{2} & -\frac{\sqrt{3}}{2} \end{pmatrix} \begin{pmatrix} I_a \\ I_b \\ I_c \end{pmatrix} \tag{15}$$

After transforming the signals to α-β coordinates using Equations (14) and (15), the instantaneous active and reactive powers of the loads are calculated using Equation (16).

$$\begin{pmatrix} p_L \\ q_L \end{pmatrix} = \begin{pmatrix} V_\alpha & V_\beta \\ V_\beta & -V_\alpha \end{pmatrix} \begin{pmatrix} I_{L\alpha} \\ I_{L\beta} \end{pmatrix} \tag{16}$$

The two components $v_\alpha i_{L\alpha}$ and $v_\beta i_{L\beta}$ constitute the instantaneous real power (p) of the load and the two components $v_\alpha i_{L\beta}$ and $v_\beta i_{L\alpha}$ constitute instantaneous imaginary power (q). The real power (p) and imaginary power (q) consist of both DC and AC values and can be represented as follows:

$$p = \bar{p} + \tilde{p}$$

$$q = \bar{q} + \tilde{q}$$

The components of power $\tilde{p}$, $\tilde{q}$, and $\bar{q}$ are to be supplied by the DSTATCOM into the source for the mitigation of reactive and harmonic power. It can be affirmed that the proposed controller compensates for the reactive power and improves the power quality for any reactive power consideration of the load. From the instantaneous power, the AC and DC components are separated using low-pass filters. To sustain the voltage of the DC link to its reference value, instantaneous active power at the DC capacitor is measured as p_{Loss} using the PI controller.

$p^* = \bar{p}_l + p_{Loss}$ and $q^* = \bar{q}_l$ are computed and transformed back to the abc plane using the inverse Clarke's transformation, as in Equation (17).

$$\begin{pmatrix} i_a^* \\ i_b^* \\ i_c^* \end{pmatrix} = \sqrt{\frac{2}{3}} \begin{pmatrix} 1 & 0 \\ -\frac{1}{2} & -\frac{\sqrt{3}}{2} \\ -\frac{1}{2} & -\frac{\sqrt{3}}{2} \end{pmatrix} \begin{pmatrix} V_\alpha & V_\beta \\ V_\beta & -V_\alpha \end{pmatrix}^{-1} \begin{pmatrix} p^* \\ q^* \end{pmatrix} \quad (17)$$

As shown in Figure 5, the currents i_a^*, i_b^*, and i_c^* are used as reference signals. In a hysteresis current-controller block, the three current signals along with the currents measured at the output of SAPF are compared to generate appropriate gating pulses for the converter. The IC is connected to the AC system through a coupling inductor.

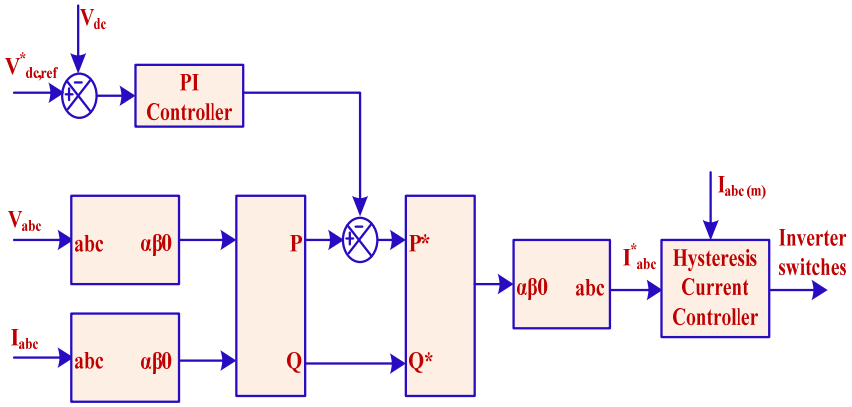

Figure 5. IC controller.

3.5. Control in Multi-Microgrid Approach

There is an increased need for the integration of multiple microgrids for enhanced stability and improved energy management. The proposed decentralized control can be adopted in the multi-microgrid approach, as depicted in Figure 6. An interlinking converter must be placed between the microgrids. Multiple autonomous systems could be coordinated by the decentralized control [42].

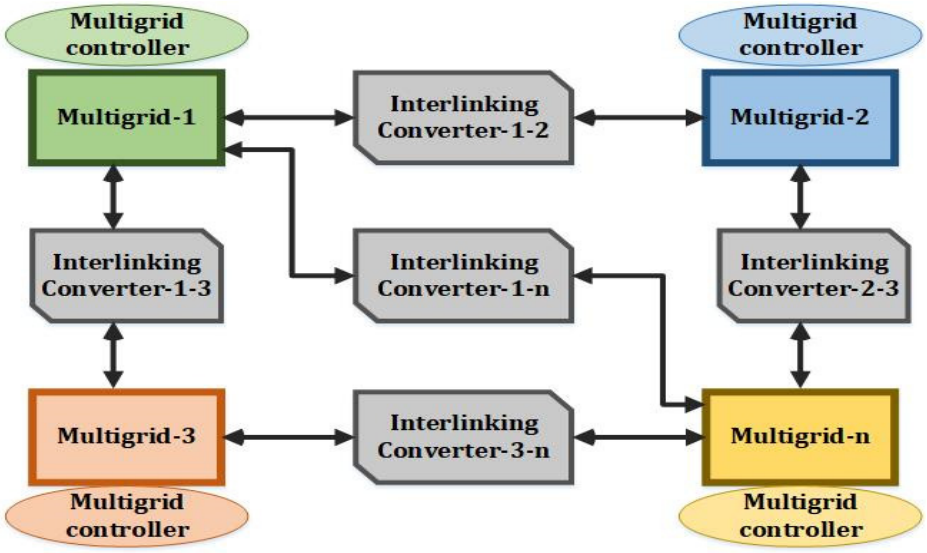

Figure 6. Decentralized control of a multi-microgrid.

4. Simulation Results and Analysis

This section deals with the simulation results of the proposed system. The designed system is modeled using the MATLAB/SIMULINK environment and the simulation results of various scenarios are examined. The simulation parameters for the proposed system are given in the Table A1: Appendix A. To show the effectiveness of the proposed control algorithm, the system is tested under different conditions, such as grid-connected and islanded modes, power transfer between the DC sub-grid and AC sub-grid through the IC, battery charging and discharging, and active filtering of the IC. The description of the modes of operation and the time period corresponding to the mode are tabulated in Table 3.

Table 3. Modes of operation of the HMG.

Sl. No.	Mode	Time Interval in Seconds	Description
1	Mode 1: grid-connected mode	0 to 1 s and 2.5 s to 4 s	AC DG units are synchronized with grid voltage and frequency (three-phase four-wire balanced system—415 V, 50 Hz)
2	Mode 2: islanded mode	1 s to 2.5 s	The system is isolated from the utility grid. The diesel generator acts as the voltage and frequency reference in the AC sub-grid. Non-critical loads of DC and AC sub-grids are turned off.
3	Mode 3: battery-charging mode	4 s to 5 s	The load in the DC sub-grid is lesser than the DG unit's generation and the battery gets charged.
4	Mode 4: DC -o-AC power-flow mode	5 s to 6 s	Power transfer takes place from the DC to the AC sub-grid. The battery is presumed to be fully charged.

4.1. Mode 1: Grid-Connected Mode

In this mode, AC DG units are synchronized with the grid voltage and frequency (415 V_{rms} and 50 Hz). The DC sub-grid consists of 25 kW loads. In the DC sub-grid, the PV array generates a power of 6.6 kW and the PMSG wind turbine generates a power of 10 kW, the battery supplies power of 4.6 kW, and the remaining 3.8 kW power for the DC load is supplied by the AC sub-grid through the IC. It is observed between 0 s < t < 1 s in the simulation results, as shown in Figure 7.

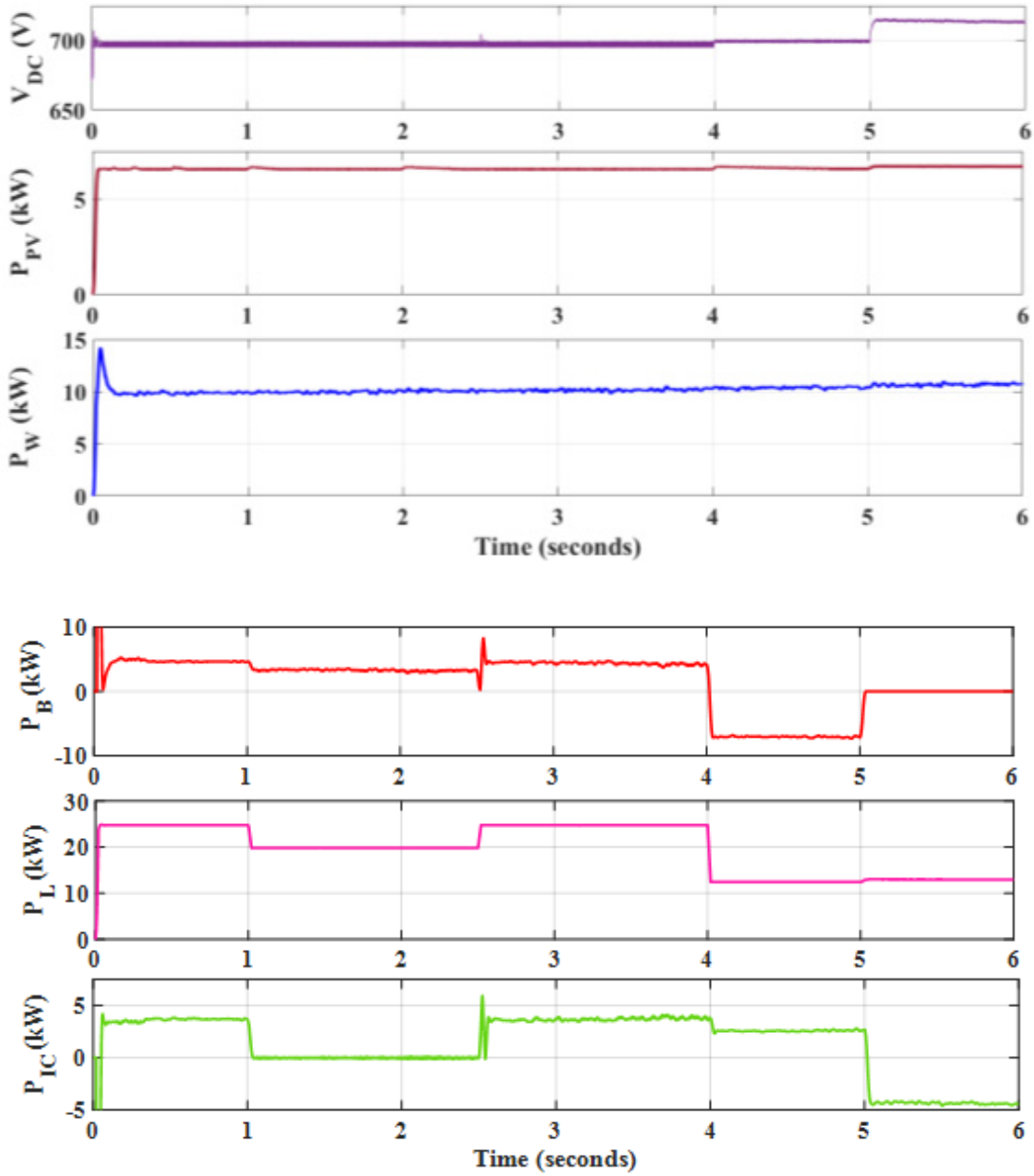

Figure 7. DC sub-grid voltage and power at rated load in the HMG.

The AC sub-grid consists of non-linear loads of 72.5 kW active power and 12 kVAr reactive power, and the IC transfers active power of 3.8 kW to the DC sub-grid. In the AC sub-grid, the PMSG WT generates an active power of 10 kW and the fuel cell generates active power of 26 kW. The remaining active power requirement of 40.3 kW is absorbed from the grid, as shown in Figure 8 for the time period 0 s < t < 1 s. Since the IC is also designed to act as a virtual APF, the IC injects reactive power to maintain the power factor and eliminate harmonics. Thus, a reactive power of 12 kVAr is injected into the AC sub grid by the IC. Of this, 11 kVAr is used to serve the non-linear loads of 11 kVAr, and the excess 1 kVAr reactive power is injected back into the grid, which is shown in Figure 9 in the time period 0 s < t < 1 s. The efficient power-sharing among the DC and AC microgrids by the proposed control is inferred from the power-sharing details projected in Table 4 for the rated load connected to the sub-grids. In the DC sub-grid, the power from the PV and wind turbine is utilized effectively and the excess power demand is supported by the

battery and the AC grid through the IC. The nonlinear loads in the AC sub-grid are supported by the power of the wind turbine and fuel cell. The excess demand in the AC grid is supplied by the power from the grid. The IC converter takes care of the reactive power demand and injects reactive power into the grid for power-quality improvement.

Table 4. Power sharing of the HMG for various modes of operation at rated load.

Mode	Details of Load Connected	P_{PV^*} (kW)	$P_{WT\text{-}DC^*}$ (kW)	P_{B^*} (kW)	P_{IC^*} (kW)	$P_{WT\text{-}AC^*}$ (kW)	P_{FC^*} (kW)	P_{G^*} (kW)	P_{DG^*} (kW)
Mode 1	DC sub grid load—25 kW	6.6	10	4.6	3.8		-	-	-
	Non-linear loads in AC sub grid—P = 72.5 kW	-	-	-	−3.8	10	26	40.3	-
	Non-linear loads in AC sub-grid—Q = 11 kVAr	-	-	-	12	-	-	-	−1
Mode 2	DC sub-grid critical load—20 kW	6.6	10	3.4	-	-	-	-	-
	Non-linear critical loads in AC sub-grid—P = 50 kW	-	-	-	-	10	26	-	14
	Non-linear critical loads in AC sub-grid—Q = 2.5 kVAr	-	-	-	-	-	-	-	2.5
Mode 3	DC sub-grid load—12.5 kW	6.6	10	−7	2.9		-	-	-
	Non-linear loads in AC sub-grid—P = 72.5 kW	-	-	-	−2.9	10	26	39.4	-
Mode 4	DC sub-grid load—12.5 kW	6.6	10	-	−4.1	-	-	-	-
	Non-linear loads in AC sub-grid—P = 72.5 kW				4.1	10	26	32.4	-

P_{PV^*}—photovoltaic, $P_{WT\text{-}DC^*}$—wind turbine in DC grid, P_{B^*}—battery, P_{IC^*}—interlinking converter, $P_{WT\text{-}AC^*}$—wind turbine in AC grid, P_{FC^*}—fuel cell, P_{G^*}—grid, P_{DG^*}—diesel generator.

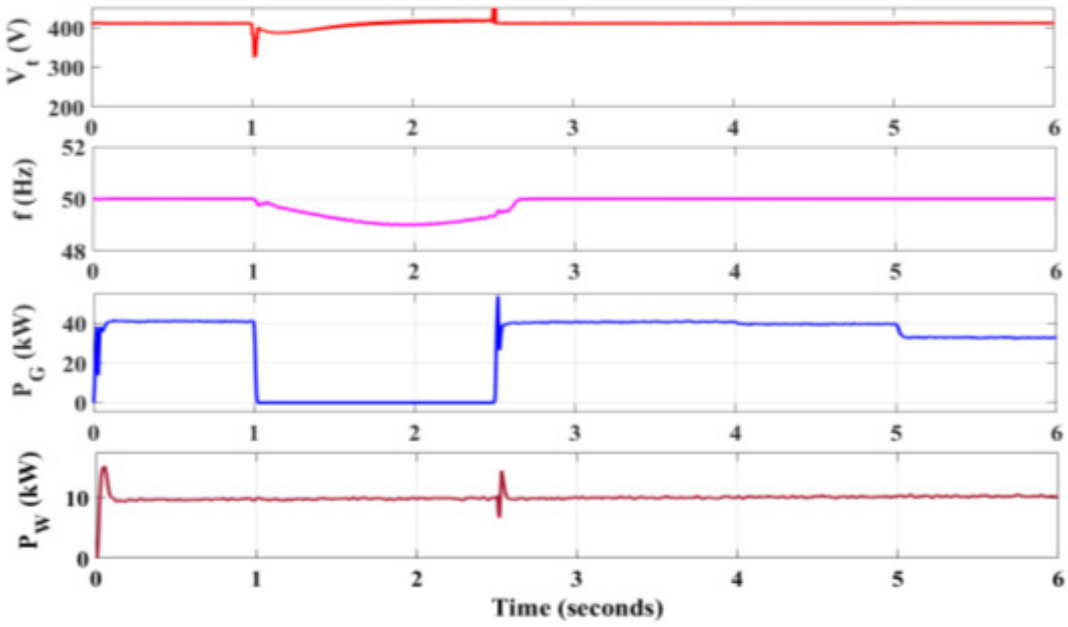

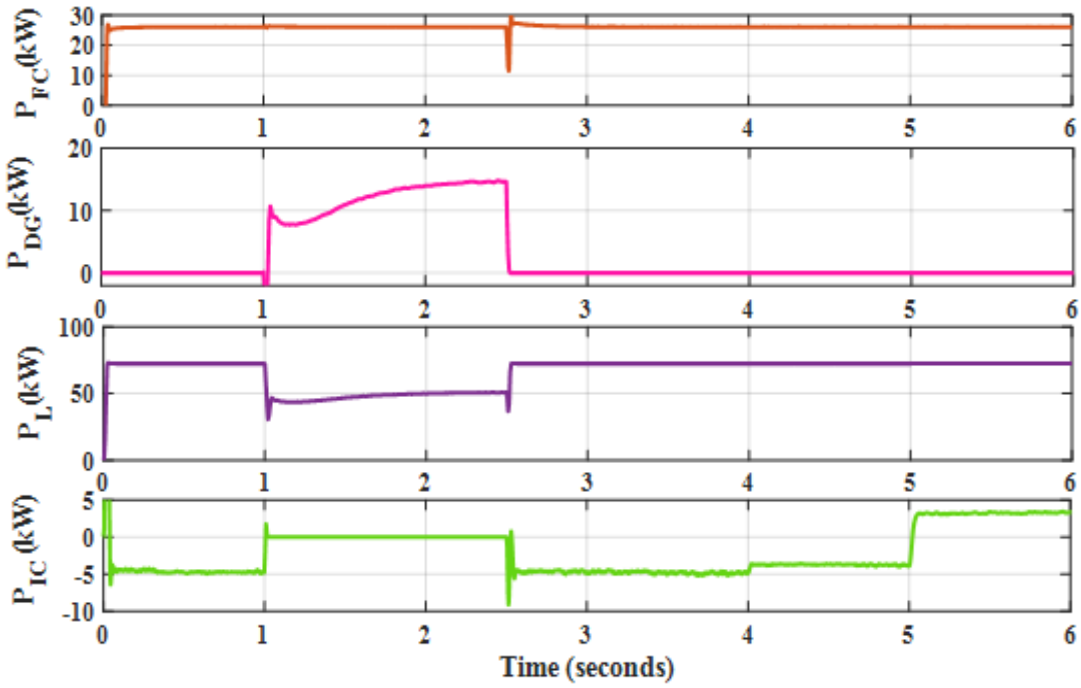

Figure 8. AC sub-grid Vrms, frequency, and active power at rated load in the HMG.

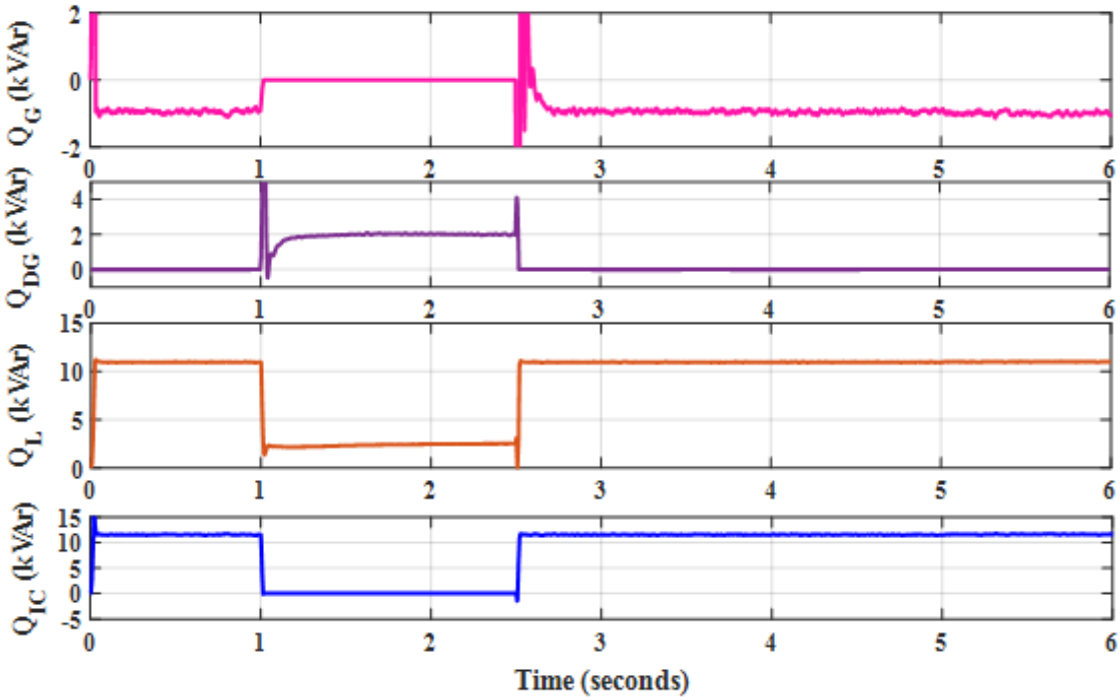

Figure 9. AC sub-grid reactive power at rated load in the HMG.

4.2. Mode 2: Islanded Mode

During this mode of operation, the system is isolated from the utility grid by the opening of STS at t = 1 s. In this mode, a diesel generator is connected at the PCC of the AC sub-grid, which acts as the voltage and frequency reference for other DG units in the AC sub-grid. During this mode of operation, the IC is disconnected by opening the STS and non-critical loads are turned off in both the DC and AC sub-grids. In the DC sub-grid, the loads are reduced to 20 kW, and the PMSG WT and PV arrays generate a power of 10

kW and 6.6 kW, respectively. The remaining 3.4 kW is supplied by the battery, which is shown in Figure 7 in the time period of 1 s < t < 2.5 s.

In the AC sub-grid, the loads are reduced to 50 kW and 2.5 kVAr. The PMSG WT and fuel cell generate active power of 10 kW and 26 kW, respectively, and the remaining 14 kW active power demand is met by a diesel generator. Since the IC is disconnected, the reactive power of 2.5 kVAr for the load demand is met by the diesel generator, which is shown in Figures 8 and 9 in the time period of 1 s< t < 2.5 s. The details of power-sharing among AC and DC microgrids are tabulated in Table 4. The seamless transfer from grid-connected mode to islanded mode is visualized at 2.5 s in Figures 7–9. The renewable sources are effectively utilized for meeting the power demand and the diesel generator is used to meet only the excess power demand during the standalone mode.

At t = 2.5 s, the STS across the grid is closed and the grid is connected to the system. At once, the AC DG unit references are changed to grid voltage and frequency, and the system transfers from islanded mode to grid-connected mode seamlessly. During the time interval 2.5 s < t < 4 s, the system operates the same as in mode 1.

4.3. Mode 3: Battery-Charging Mode

In this mode, the load in the DC sub-grid reduces to 12.5 kW at t = 4 s. The total power generation in the DC sub-grid is 16.6 kW. As the DC demand is lower than the DC DG unit generation, the battery starts charging by consuming a power of 7 kW. The remaining 2.9 kW power for battery charging is obtained from the AC sub-grid through the IC, which is shown in Figure 7 in the time interval of 4 s < t <5 s.

During this mode in the AC sub-grid, the load and DG unit power generation is the same as in mode 1 except that the power obtained from the grid is reduced to 39.4 kW as the power exchange to the DC sub-grid is reduced to 2.9 kW. The reactive power flow remains the same as in mode 1, which is shown in Figures 8 and 9 in the time interval of 4 s < t < 5 s.

4.4. Mode 4: DC-to-AC Power Flow

During this mode of operation, the power transfer from the DC sub-grid to the AC sub-grid is realized. At t = 5 s, the battery is presumed to be charged fully. As the load in DC sub-grid is 12.5 kW and the generation of power is 16.6 kW, the excess power of 4.1 kW is transferred to the AC sub-grid through the IC, which is shown in Figure 7 in the time interval of 5 s < t <6 s.

In the AC sub-grid, the loading and generation of DG units remain the same as in mode 1. The excess power of 4.1 kW from the DC is injected into the AC, and the power consumed from the grid is reduced to 32.4 kW from 39.4 kW in mode 3. The reactive power flow remains the same as in mode 1, which is shown in Figures 8 and 9 in the time interval of 5 s < t <6 s.

4.5. Virtual APF

The three-phase AC grid and load voltage, grid, and load current are shown in Figure 10. From Figure 10, it is observed that at t =1 s, the grid is disconnected. Thus, the grid current and voltage become zero at that point. The load voltage and current remain sinusoidal. The voltage is 415 V_{rms} and the current amplitude varies in the grid and islanded mode due to the change in load.

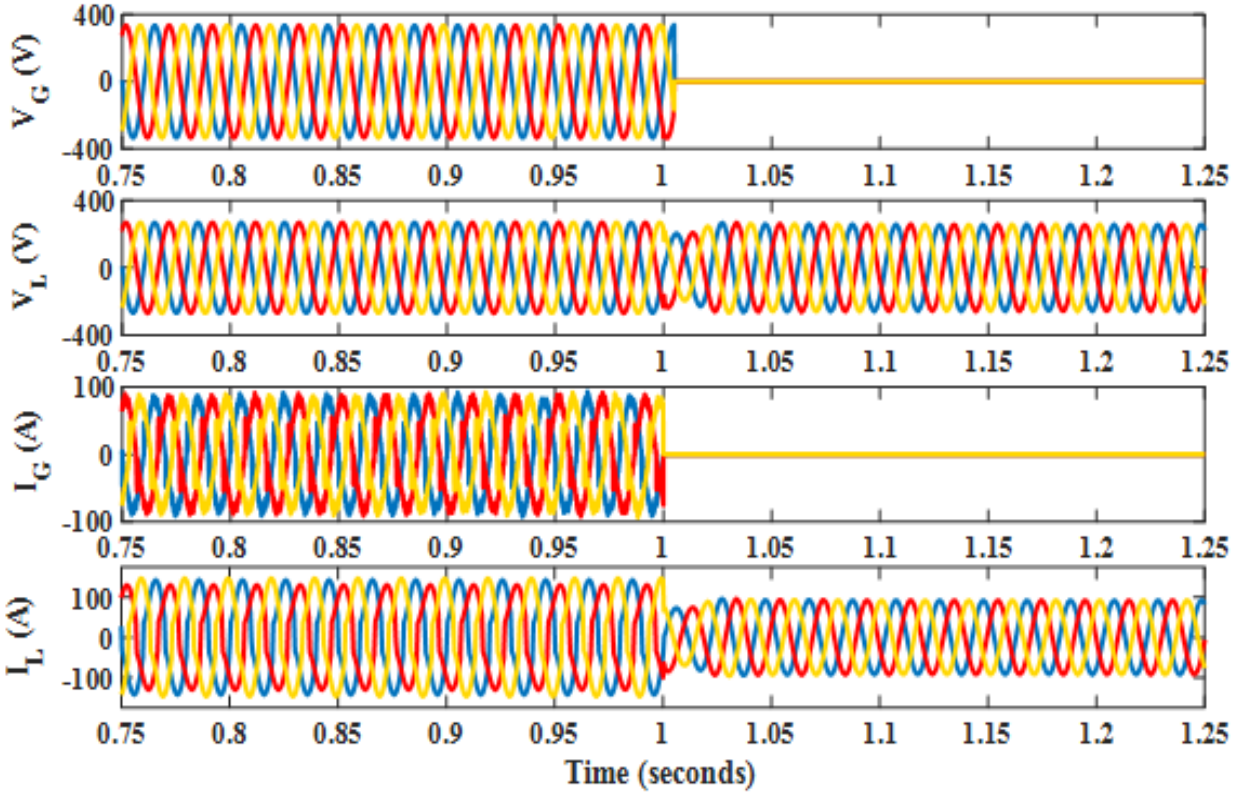

Figure 10. AC sub-grid grid voltage, load voltage, grid current, and load current.

From Figure 10, it is also observed that during the grid-connected mode, the AC load current is distorted due to the harmonics of non-linear load, but the grid current remains sinusoidal with harmonics at less than 5% due to the compensation by the IC acting as a virtual APF. Table 5 shows the %THD in the AC sub-grid voltage, grid current, and load current when the IC is used as an APF and power-exchange converter. From the tabulation in Table 5, it is evident that the IC performs as an APF to maintain the THD of the grid current within 5% even when the load-current THD is higher due to the non-linear loads of the AC sub-grid. Figures 11–13 show the %THD of the R_{ph} load current, R_{ph} grid current, and R_{ph} voltage, respectively. Figure 14 shows the performance of the IC in maintaining the THD of the grid current when it is operated as an APF and power-exchange converter. The superior performance of the IC as an APF in maintaining the THD below 5% is evident from the chart in Figure 14.

Table 5. Performance comparison of the IC as APF and power-exchange converter.

Phase	IC as APF in HMG			IC for Power Exchange in HMG		
	AC Sub-grid Voltage	Grid Current	Load Current	AC Sub-grid Voltage	Grid Current	Load Current
	%THD	%THD	%THD	%THD	%THD	%THD
R_{ph}	0.07	4.33	14.29	7.50%	15.4	14.29
Y_{ph}	0.07	4.64	15.77	8.30%	16.2	15.77
B_{ph}	0.07	4.24	13.29	8.50%	15.9	13.29

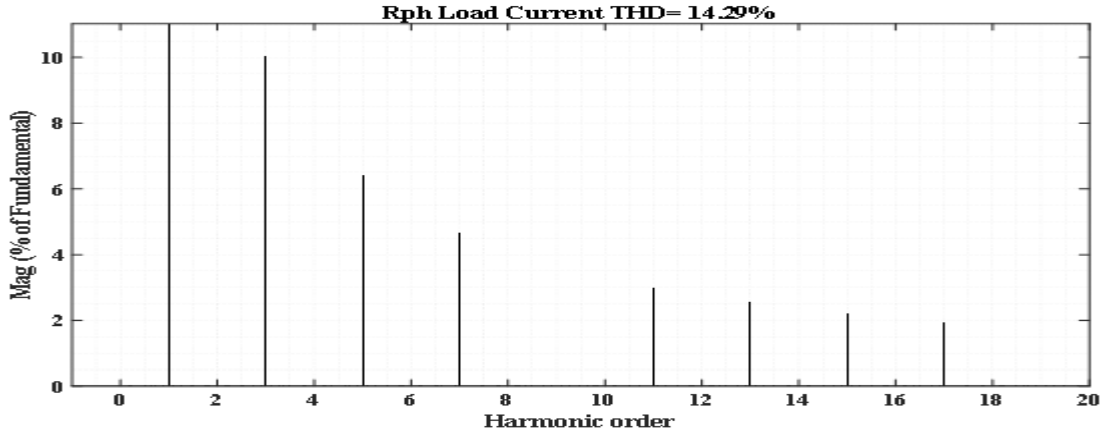

Figure 11. THD analysis of R_{ph} load current.

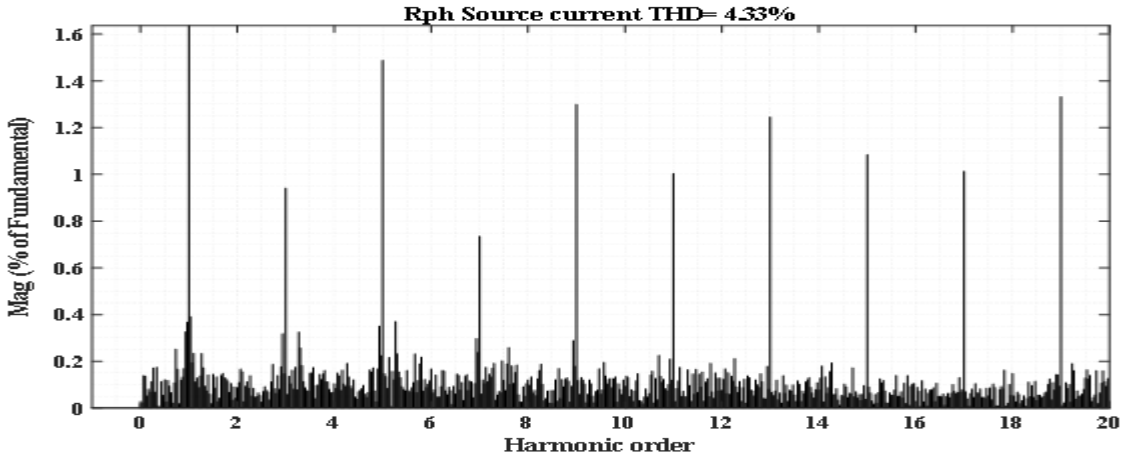

Figure 12. THD analysis of R_{ph} grid current.

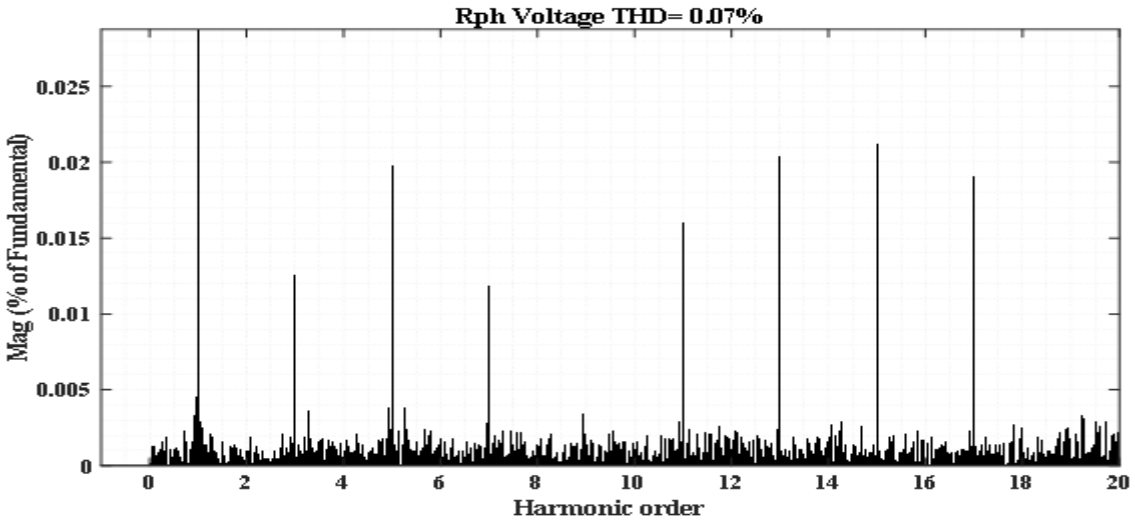

Figure 13. THD analysis of R_{ph} voltage.

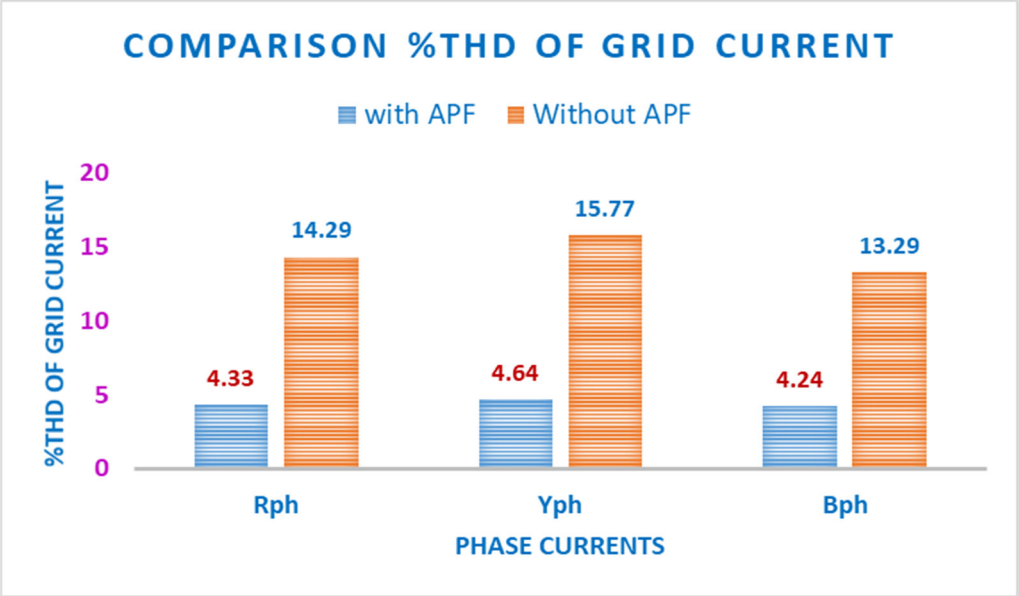

Figure 14. Comparison of %THD of grid current.

4.6. Performance of HMG with a Reduction in Load

The load on the DC microgrid is reduced by 10% and the performance of the HMG is analyzed for power-sharing, seamless transition, and power quality improvement. The details of the load connected in each mode and the power shared by each renewable energy source and energy-storage element are tabulated in Table 6. Figures 15–18 show the power in the DC sub-grid, the real power in the AC sub-grid, the reactive power in the AC sub-grid, and the grid voltage, frequency, and power flow of the battery, respectively. The details presented in Table 6 and the traces in Figures 15–18 show the efficient power-sharing of the HMG from RES. In DC MG the excess power to be supplied to the load is shared by the battery and AC sub-grid through the IC. Similarly, in the AC MG, the load is supplied from the wind turbine and fuel cell, and the additional power requirement is compensated from the grid. Even during load reduction, the IC manages the reactive power demand and improves the power quality of the grid, and the decentralized control maintains the V_{PCC} and frequency of the AC sub-grid.

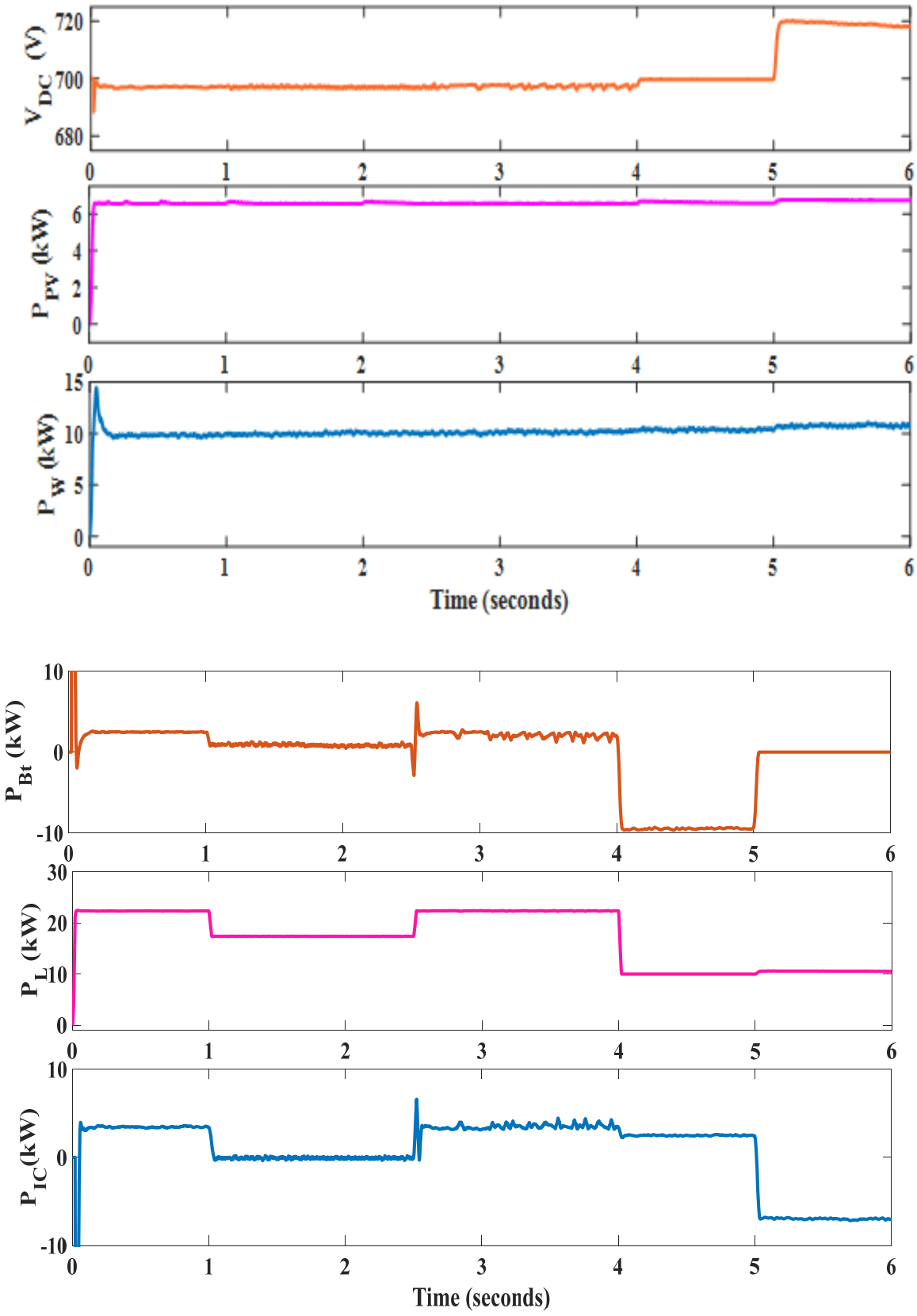

Figure 15. DC sub-grid voltage and power with 10% load reduction in the HMG.

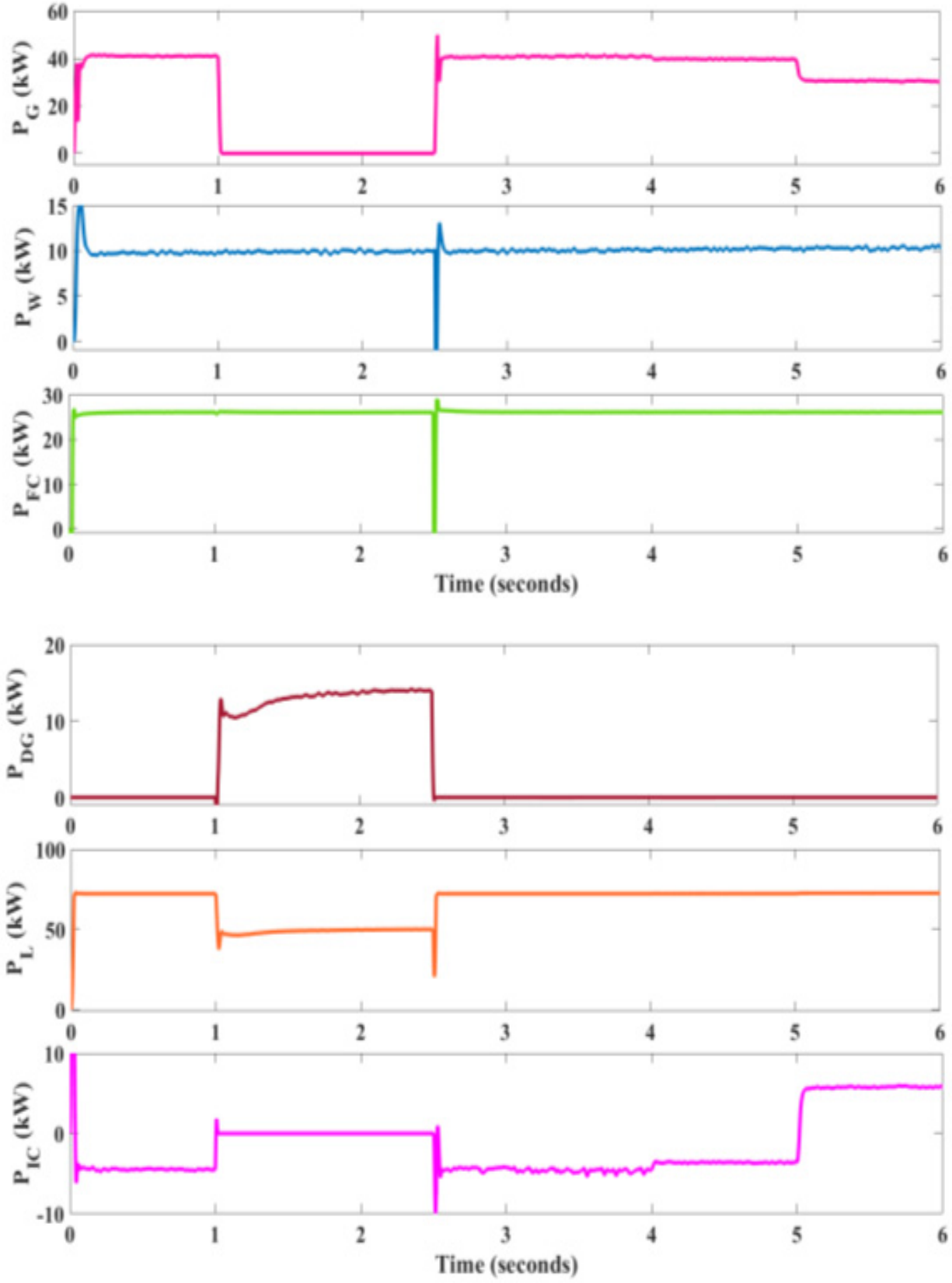

Figure 16. AC sub-grid active power with 10% load reduction in the HMG.

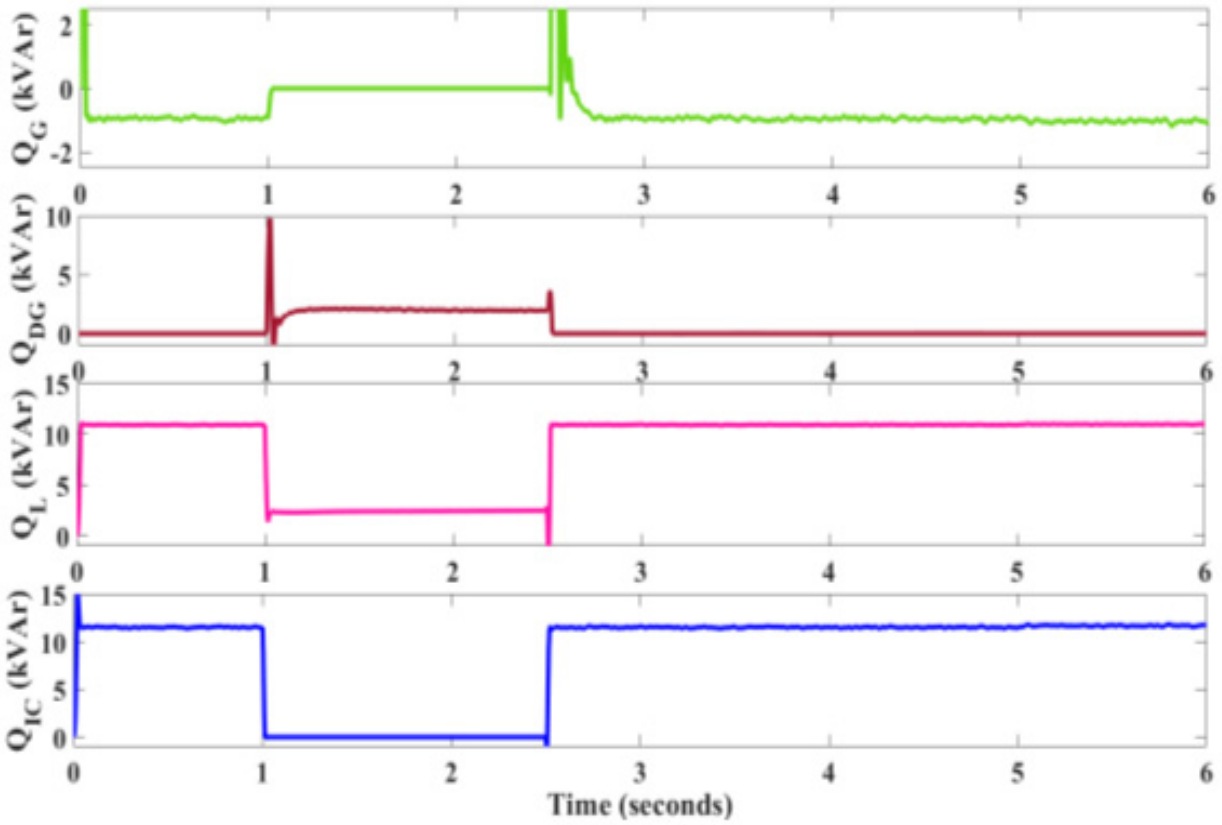

Figure 17. AC sub-grid reactive power with 10% load reduction in the HMG.

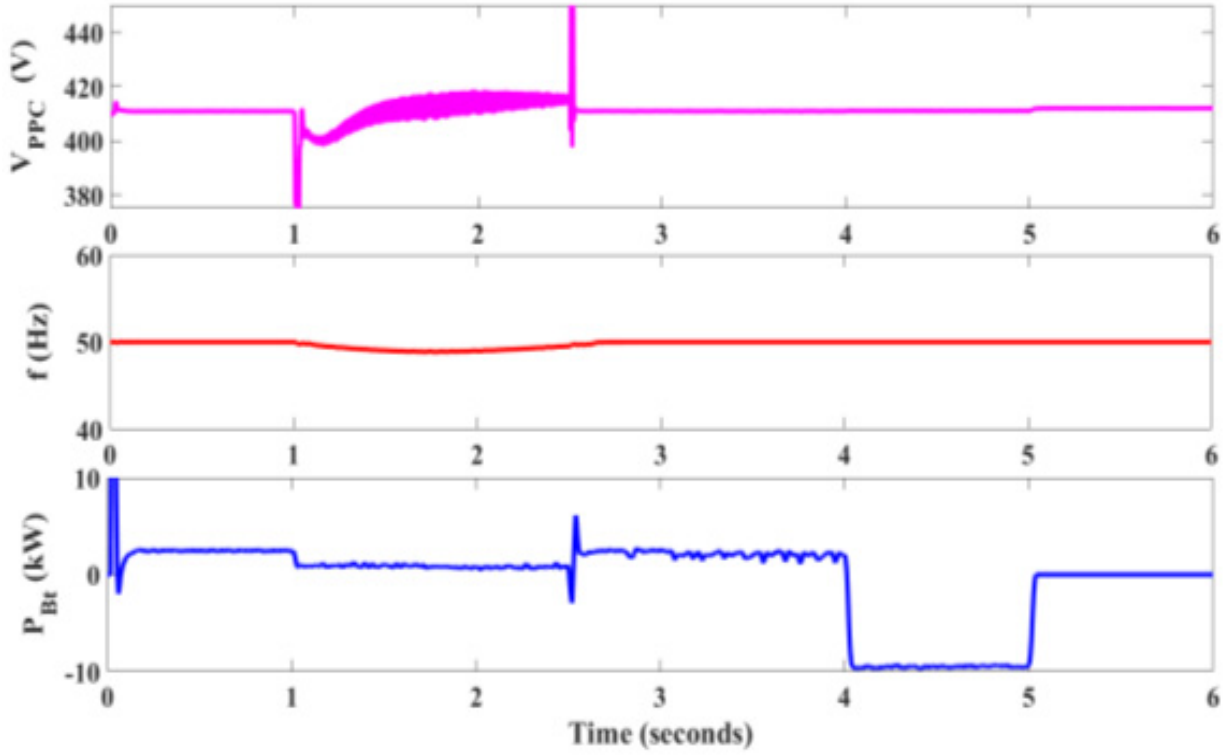

Figure 18. AC sub-grid V_{PCC}, frequency, and power flow of battery with 10% load reduction in the HMG.

Table 6. Power sharing of the HMG for various modes of operation at 10% reduction in rated load.

Mode	Details of Load Connected	P_{PV^*} (kW)	$P_{WT\text{-}DC^*}$ (kW)	P_{B^*} (kW)	P_{IC^*} (kW)	$P_{WT\text{-}AC^*}$ (kW)	P_{FC^*} (kW)	P_{G^*} (kW)	P_{DG^*} (kW)
Mode 1	DC sub-grid load—22.5 kW	6.6	10	2.5	3.4		-	-	-
	Non-linear loads in AC sub grid—P = 72.5 kW	-	-	-	−3.4	10	26	40	-
	Non-linear loads in AC sub grid—Q = 11 kVAr				12				−1
Mode 2	DC sub-grid critical load—18 kW	6.6	10	1.4	-	-	-	-	-
	Non-linear critical loads in AC sub-grid—P = 50 kW	-	-	-	-	10	26	-	14
	Non-linear critical loads in AC sub-grid—Q = 2.5 kVAr	-	-	-	-	-	-	-	2.5
Mode 3	DC sub-grid load—10 kW	6.6	10	−9	2.4		-	-	-
	Non-linear loads in AC sub grid—P = 72.5 kW	-	-	-	−2.4	10	26	38.9	-
Mode 4	DC sub-grid load—11 kW	6.6	10	-	−5.6	-	-	-	-
	Non-linear loads in AC sub-grid—P = 72.5 kW				5.6	10	26	30.9	-

P_{PV^*}—photovoltaic, $P_{WT\text{-}DC^*}$—wind turbine in DC grid, P_{B^*}—battery, P_{IC^*}—interlinking converter, $P_{WT\text{-}AC^*}$—wind turbine in AC grid, P_{FC^*}—fuel cell, P_{G^*}—grid, P_{DG^*}—diesel generator.

4.7. Performance of HMG with Increment in Load

The load on the DC microgrid is increased by 10% and the performance of the HMG is analyzed for power sharing, seamless transition, and power-quality improvement. The details of the load connected in each mode and the power shared by each renewable energy source and energy-storage element are tabulated in Table 7.

Table 7. Power sharing of the HMG for various modes of operation at 10% increment in rated load.

Mode	Details of Load Connected	P_{PV^*} (kW)	$P_{WT\text{-}DC^*}$ (kW)	P_{B^*} (kW)	P_{IC^*} (kW)	$P_{WT\text{-}AC^*}$ (kW)	P_{FC^*} (kW)	P_{G^*} (kW)	P_{DG^*} (kW)
Mode 1	DC sub-grid load—27.5 kW	6.6	10	7.1	3.8		-	-	-
	Non-linear loads in AC sub-grid—P = 72.5 kW	-	-	-	−3.8	10	26	40.3	-
	Non-linear loads in AC sub-grid—Q = 11 kVAr				12				−1
Mode 2	DC sub-grid critical load—22 kW	6.6	10	5.4	-	-	-	-	-
	Non-linear critical loads in AC sub-grid—P = 50 kW	-	-	-	-	10	26	-	14
	Non-linear critical loads in AC sub-grid—Q = 2.5 kVAr	-	-	-	-	-	-	-	2.5
Mode 3	DC sub-grid load- 12.5 kW	6.6	10	−7	2.9		-	-	-
	Non-linear loads in AC sub-grid—P = 72.5 kW	-	-	-	−2.9	10	26	39.4	-
Mode 4	DC sub-grid load—12.5 kW	6.6	10	-	−4.1	-	-	-	-
	Non-linear loads in AC sub-grid—P = 72.5 kW				4.1	10	26	32.4	-

P_{PV^*}—photovoltaic, $P_{WT\text{-}DC^*}$—wind turbine in DC grid, P_{B^*}—battery, P_{IC^*}—interlinking converter, $P_{WT\text{-}AC^*}$—wind turbine in AC grid, P_{FC^*}—fuel cell, P_{G^*}—grid, P_{DG^*}—diesel generator.

Figures 19–21 show the power in the DC sub-grid, the real power in the AC sub-grid, and the grid voltage, frequency, and power flow of the battery, respectively. The details presented in Table 7 and the traces in Figures 19–21 show the efficient power sharing of the HMG from RES. The excess power to be supplied to the load in the DC sub-grid is shared by the battery and AC sub-grid through the IC. Similarly, the load is supplied from the wind turbine and fuel cell in the AC sub-grid, and the additional power requirement is compensated from the grid. Even during load increment the IC manages the reactive power demand and improves the power quality of the grid, and the decentralized control maintains the V_{PCC} and frequency of the AC sub-grid.

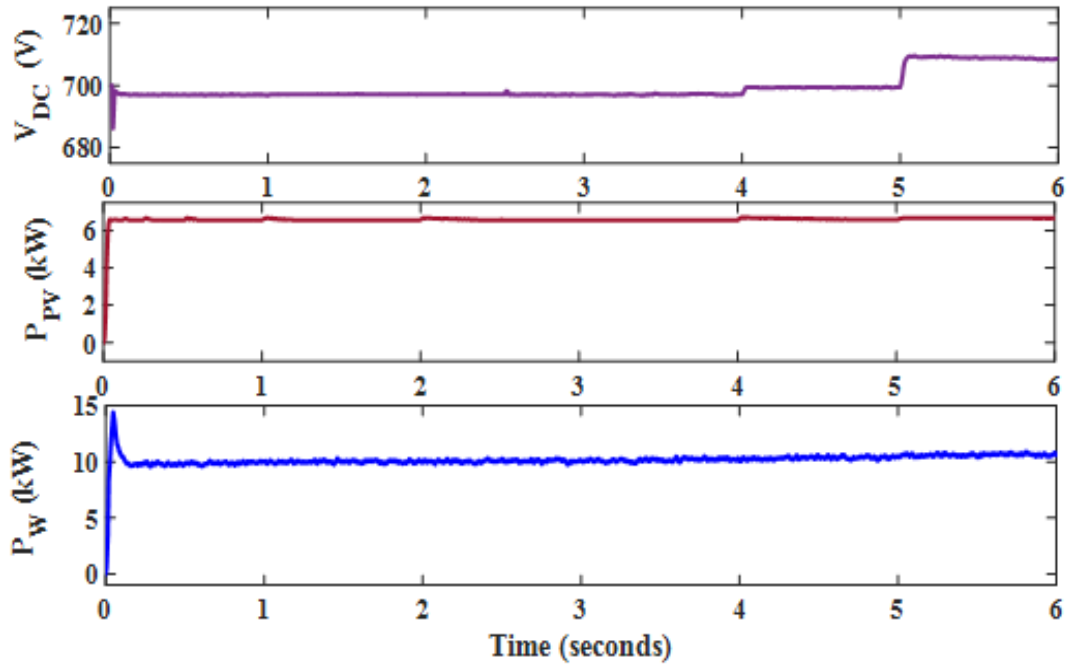

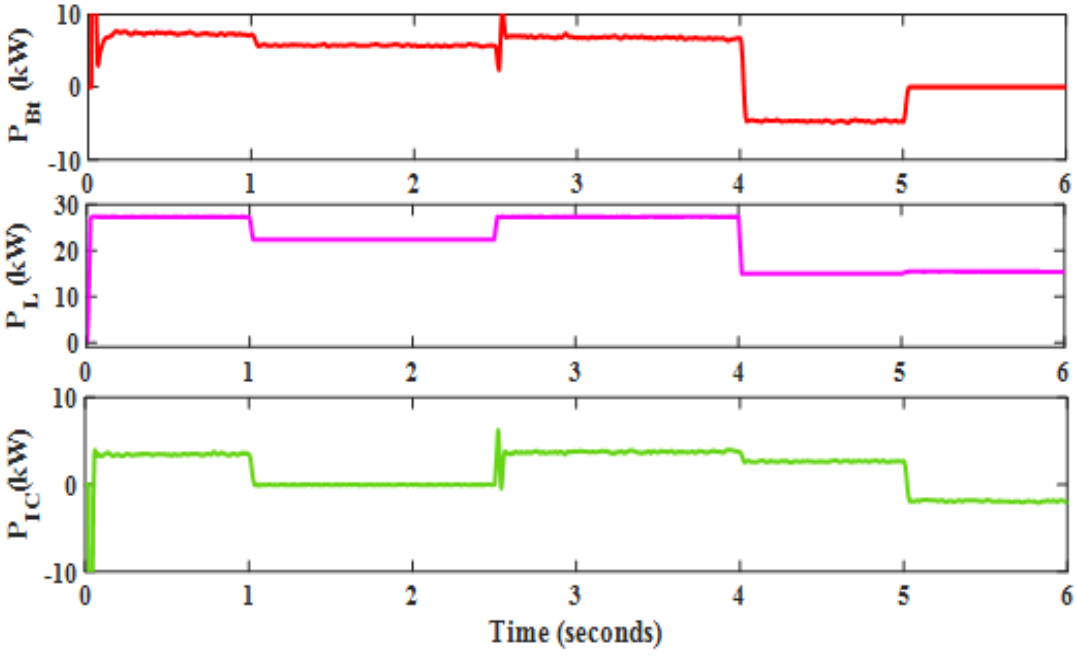

Figure 19. DC sub-grid voltage and power with 10% load increment in the HMG.

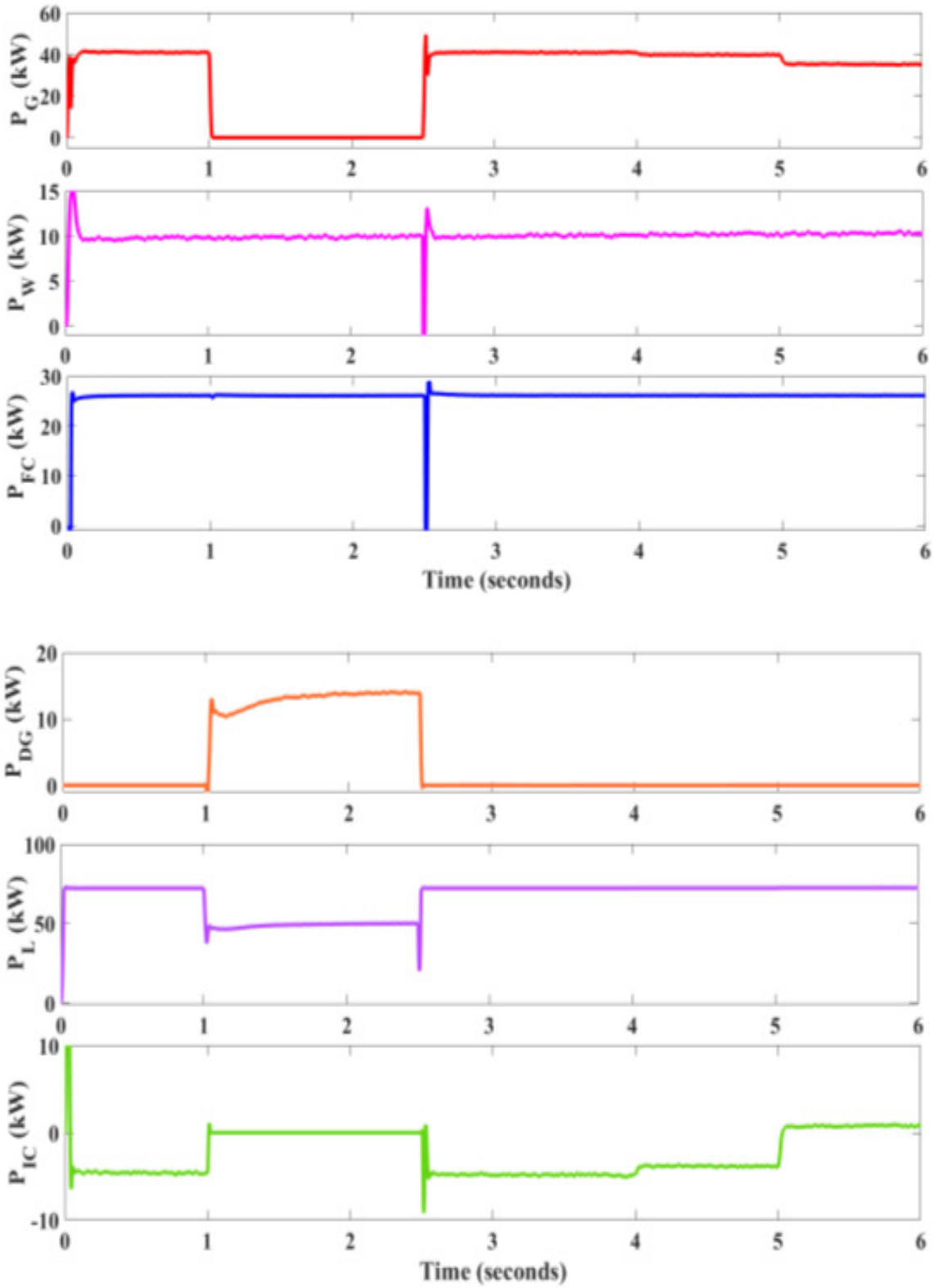

Figure 20. AC sub-grid active power with 10% load increment in the HMG.

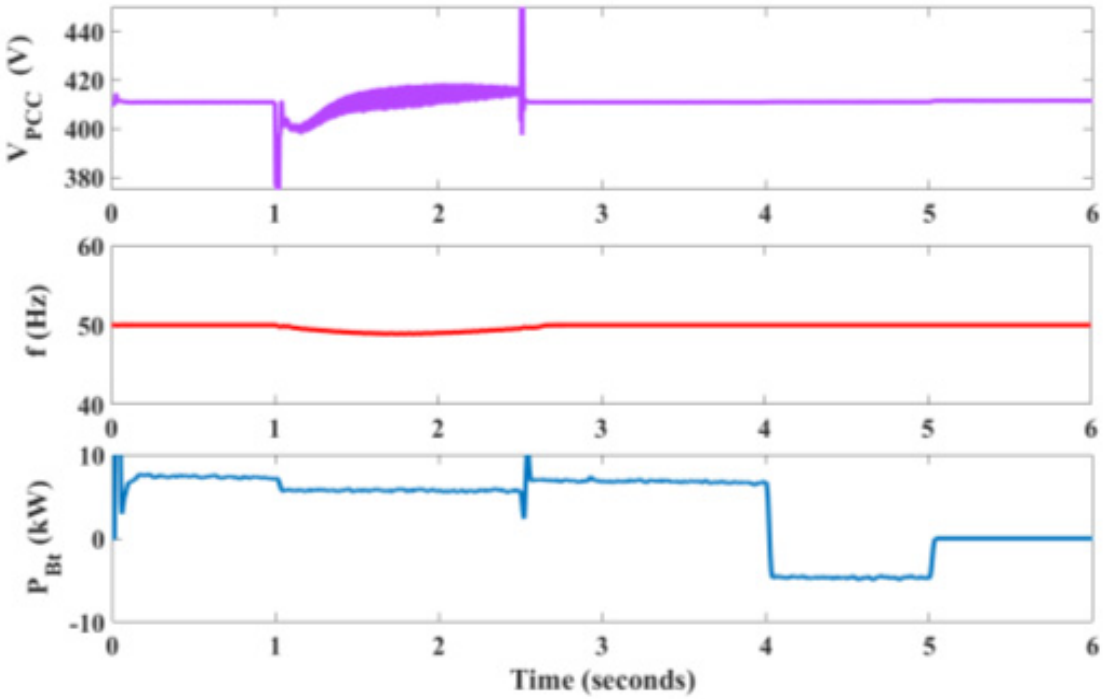

Figure 21. AC sub-grid V_{PCC}, frequency, and power flow of battery with 10% load increment in the HMG.

5. Conclusions

The proposed HMG system is modeled and simulated. The simulation results verify that various types of renewables can be integrated efficiently into the AC and DC microgrid system with maximum power extraction. The system can effectively utilize power from renewable sources during load demand or store power and utilize it during islanded mode. Apart from power exchange between AC and DC microgrids, the modified control algorithm enables the IC to act as a virtual APF for improving power quality during unbalanced and non-linear load conditions. The %THD of the grid current is maintained at less than 5%, as specified by IEEE519 standards. The decentralized control supports the seamless switching between grid-connected and islanded modes. The system is stable during all modes of operation, meeting all load demands at reference voltages and frequency. The HMG with the proposed control performs efficiently with variations in load in terms of power sharing, seamless transition, power-quality improvement, maintenance of V_{PCC}, and frequency of the AC grid.

The key findings of the paper are:

- The proposed controller efficiently coordinates the AC/DC hybrid microgrid in all four modes of operation.
- The required power is transferred between the AC and DC microgrid via the interlinking converter. With an energy-storage system, the power exchange between the microgrids is efficiently managed by the controller and only the excess power demand is obtained from the utility grid.
- The modified control technique for the interlinking converter improves the power quality under unbalanced and non-linear load conditions.
- The interlinking converter supports AC/DC voltage bidirectionally during the islanded mode of operation. This reduces the need for additional voltage sources.
- The proposed controller helps in the seamless transfer between grid-connected and isolated modes.

The future works to be carried out are:

- The proposed controller can be extended to a multi-microgrid approach.
- The multi-parallel interlinking converter can be utilized in place of the interlinking converter, and an analysis can be carried out.
- The proposed controller can be applied for real-time applications.
- Economic analysis and the impact of the proposed microgrid on the present microgrid setup can be analyzed through HOMER software.
- Degradation of the hybrid components can be included in the analysis.

Author Contributions: Formal analysis, J.J.; Methodology, J.J.; Supervision, T.S.; Validation, M.S., N.P. and T.S.; Writing—original draft, M.S.; Writing—review & editing, N.P. All authors have read and agreed to the published version of the manuscript.

Funding: This research received no external funding.

Institutional Review Board Statement: Not applicable.

Informed Consent Statement: Not applicable.

Data Availability Statement: Data sharing is not applicable to this article.

Acknowledgments: The authors would like to express their gratitude to the management of SASTRA Deemed University for providing renewable energy lab facilities.

Conflicts of Interest: The authors declare no conflict of interest.

Abbreviations

APF	Active power filter
BESS	Battery energy storage system
DG	Distributed generation
HMG	Hybrid microgrid
IC	Interlinking converter
IRPT	Instantaneous reactive power theory
MG	Microgrid
MGCC	Microgrid centralized controller
MPPT	Maximum power point tracking
PCC	Point of common coupling
PI	Proportional integral
PLL	Phase locked loop
PMSG	Permanent magnet synchronous generator
P&O	Perturb and observe
RES	Renewable energy sources
STS	Static transfer switch
THD	Total harmonic distortion
WT	Wind turbine

Appendix A

Table A1. Simulation parameters for the proposed system.

Utility Grid	
Three-phase four-wire system with balanced voltages	415 V, 50 Hz
Source impedance	R = 1 Ω, L= 6 mH
PMSG Wind Turbine	
Nominal mechanical power—P_m	12 kW
Nominal generator electrical power—P_g	12/0.9 kVA
Nominal wind speed—V_m	12 m/s
Maximum power at base speed	0.8 (p.u)
Wind Turbine Inverter	
DC link voltage—V_{DC}	677.49~700 V
DC link capacitor—C_{DC}	4685 uF~4700 uF

Coupling inductor—(R + L)	0.026 + 8.22 mH
Ripple filter—(P + Q)	20 W + 1 kVAr
Fuel Cell	
Voltage at (0 A, 1 A)	(450.442.5) V
Nominal current—I_{nom}	40 A
Nominal voltage—V_{nom}	350 V
Maximum current—I_{end}	140 A
Power obtained—P_{obt}	27 kW
Boost Converter	
Inductor—L	3.9 mH
Capacitor—C	70 μF
Switching frequency—f_s	10 kHz
Duty cycle—D	50%
Buck–Boost Converter	
Inductor—L	3 mH
Capacitor—C	70 μF
Switching frequency—f_s	10 kHz
Duty cycle—D	50%
Fuel Cell Inverter	
DC link voltage—V_{DC}	677.49~700 V
DC link capacitor—C_{DC}	4685~4700 μF
Coupling inductor—(R + L)	0.01722 + 5.48 mH
Ripple filter—(P + Q)	30 W + 1.5 kVAr

References

1. Amirthalingam, M. A Novel Technology utilizing Renewable energies to mitigate air pollution, global warming & climate change. In Proceedings of the 1st International Conference on the Developments in Renewable Energy Technology (ICDRET), Dhaka, Bangladesh, 17–19 December 2009; pp. 1–3.
2. Bauer, N.; Mouratiadou, I.; Luderer, G.; Baumstark, L.; Brecha, R.J.; Edenhofer, O.; Kriegler, E. Global fossil energy markets and climate change mitigation—An analysis with REMIND. *Clim. Chang.* **2016**, *136*, 69–82.
3. Tiwari, S.K.; Singh, B.; Goel, P.K. Design and control of micro-grid fed by renewable energy generating sources. *IEEE Trans. Ind. Appl.* **2018**, *54*, 2041–2050.
4. Bose, B.K. Global Energy Scenario and Impact of Power Electronics in 21st Century. *IEEE Trans. Ind. Electron.* **2013**, *60*, 2638–2651.
5. Singh, B.; Pathak, G.; Panigrahi, B.K. Seamless Transfer of Renewable-Based Microgrid Between Utility Grid and Diesel Generator. *IEEE Trans. Power Electron.* **2018**, *33*, 8427–8437.
6. Ochs, D.S.; Mirafzal, B.; Sotoodeh, P. A Method of Seamless Transitions Between Grid-Tied and Stand-Alone Modes of Operation for Utility-Interactive Three-Phase Inverters. *IEEE Trans. Ind. Appl.* **2014**, *50*, 1934–1941.
7. Tang, F.; Guerrero, J.M.; Vasquez, J.C.; Wu, D.; Meng, L. Distributed Active Synchronization Strategy for Microgrid Seamless Reconnection to the Grid Under Unbalance and Harmonic Distortion. *IEEE Trans. Smart Grid* **2015**, *6*, 2757–2769.
8. Olivares, D.E.; Mehrizi-Sani, A.; Etemadi, A.H.; Cañizares, C.A.; Iravani, R.; Kazerani, M.; Hajimiragha, A.H.; Gomis-Bellmunt, O.; Saeedifard, M.; Palma-Behnke, R.; et al. Trends in Microgrid Control. *IEEE Trans. Smart Grid* **2014**, *5*, 1905–1919.
9. Fathima, H.; Prabaharan, N.; Palanisamy, K.; Kalam, A.; Mekhilef, S.; Justo, J.J. *Hybrid-Renewable Energy Systems in Microgrids: Integration, Developments and Control*; Woodhead Publishing: Thorston, UK, 2018.
10. Pannala, S.; Patari, N.; Srivastava, A.K.; Padhy, N.P. Effective Control and Management Scheme for Isolated and Grid Connected DC Microgrid. *IEEE Trans. Ind. Appl.* **2020**, *56*, 6767–6780.
11. Rezkallah, M.; Chandra, A.; Singh, B.; Singh, S. Microgrid: Configurations, Control and Applications. *IEEE Trans. Smart Grid* **2019**, *10*, 1290–1302.
12. Liu, X.; Wang, P.; Loh, P.C. A Hybrid AC/DC Microgrid and Its Coordination Control. *IEEE Trans. Smart Grid* **2011**, *2*, 278–286.
13. Li, H.; Li, Y.; Guerrero, J.M.; Cao, Y. AComprehensive Inertial Control Strategy for Hybrid AC/DC Microgrid with Distributed Generations. *IEEE Trans. Smart Grid* **2020**, *11*, 1737–1747.
14. Zolfaghari, M.; Gharehpetian, G.B.; Shafie-khan, M.; Catalao, J.P.S. Comprehensive review on the strategies for controlling the interconnection of AC and DC microgrids. *Int. J. Electr. Power Energy Syst.* **2021**, *136*, 107742.

15. Wang, L.; Fu, X.; Wong, Ma. Operation and Control of a Hybrid Coupled Interlinking Converter for Hybrid AC/Low Voltage DC Microgrids. *IEEE Trans. Ind. Electron.* **2021**, *68*, 7104–7114.
16. Phan, D.; Lee, H. Interlinking Converter to Improve Power Quality in Hybrid AC–DC Microgrids With Nonlinear Loads. *IEEE J. Emerg. Sel. Top. Power Electron.* **2019**, *7*, 1959–1968.
17. Hussain, M.N.; Melath, G.; Agarwal, V. An Active Damping Technique for PI and Predictive Controllers of an Interlinking Converter in an Islanded Hybrid Microgrid. *IEEE Trans. Power Electron.* **2021**, *36*, 5521–5529.
18. Shoeb, M.A.; Shahnia, F.; Shafiullah, G.M. A Multilayer and Event-Triggered Voltage and Frequency Management Technique for Microgrid's Central Controller Considering Operational and Sustainability Aspects. *IEEE Trans. Smart Grid* **2019**, *10*, 5136–5151.
19. Jha, S.; Hussain, I.; Singh, B.; Mishra, S. Optimal operation of PV-DG-battery based microgrid with power quality conditioner. *IET Renew. Power Gener.* **2019**, *13*, 418–426.
20. Jayachandran, J.; Sachithanandam, R.M. Neural network-based control algorithm for DSTATCOM under non-ideal source voltage and varying load conditions. *Can. J. Electr. Comput. Eng.* **2015**, *38*, 307–317.
21. Brandao, D.I.; Santos, R.P.d.; Silva, W.W.A.G.; Oliveira, T.R.; Donoso-Garcia, P.F. Model-Free Energy Management System for Hybrid Alternating Current/Direct Current Microgrids. *IEEE Trans. Ind. Electron.* **2021**, *68*, 3982–3991.
22. IEEE Recommended Practice and Requirements for Harmonic Control in Electric Power Systems; In *IEEE Std 519-2014 (Revision of IEEE Std 519-1992)*; IEEE: Piscataway, NJ, USA, 11 June 2014; pp. 1–29.
23. Jayachandran, J.; Sachithanandam, R.M. Performance investigation of artificial intelligence-based controller for three-phase four-leg shunt active filter. *Front. Energy* **2015**, *9*, 446–460.
24. Malathi, S.; Jayachandran, J. FPGA Implementation of NN based LMS-LMF Control Algorithm in DSTATCOM for Power Quality Improvement. *Control. Eng. Pract.* **2020**, *98*, 104378.
25. Kaur, S.; Dwivedi, B. Power quality issues and their mitigation techniques in microgrid system-a review. In Proceedings of the 7th India International Conference on Power Electronics (IICPE), Patiala, India, 17–19 November 2016; pp. 1–4.
26. Chang, J,-W.; Lee, G.-S.; Moon, S.-I.; Hwang, P.-I. A Novel Distributed Control Method for Interlinking Converters in an Islanded Hybrid AC/DC Microgrid. *IEEE Trans. Smart Grid* **2021**, *12*, 3765–3779.
27. Bhim, S.; Chandra, A.; Al-Haddad, K. *Power Quality: Problems and Mitigation Techniques*; John Wiley & Sons: Hoboken, NJ, USA, 2014.
28. Malathi, S.; Sachithanandam, R.M.; Jayachandran, J. Performance comparison of neural network based multi output SMPS with improved power quality and voltage regulation. *Control Eng. Appl. Inform.* **2018**, *20*, 86–97.
29. Khederzadeh, M.; Sadeghi, M. Virtual active power filter: A notable feature for hybrid ac/dc microgrids. *IET Gener. Transm. Distrib.* **2016**, *10*, 3539–3546.
30. Shafiullah, G.M.; Oo, A.M.T.; Ali, A.B.M.S.; Jarvis, D.; Wolfs, P. Economic Analysis of Hybrid Renewable Model for Subtropical Climate. *Int. J. Therm. Environ. Eng.* **2010**, *1*, 57–65.
31. Shafiullah, G.M.; Arif, M.T.; Oo, A.M.T. Mitigation strategies to minimize potential technical challenges of renewable energy integration. *Sustain. Energy Technol. Assess.* 2018. 25, 24-42.
32. Khomsi, C.; Bouzid, M.; Champenois, G.; Jelassi, K. Improvement of the Power Quality in Single Phase Grid Connected Photovoltaic System Supplying Nonlinear Load. In *Advanced Technologies for Solar Photovoltaics Energy Systems*; Motahhir, S., Eltamaly, A.M., Eds.; Green Energy and Technology; Springer: Cham, Switzerland, 2021. https://doi.org/10.1007/978-3-030-64565-6_13.
33. Eltamaly, A.M. A novel musical chairs algorithm applied for MPPT of PV systems. *Renew. Sustain. Energy Rev.* **2021**, *146*, 111135.
34. Liu, Q.; Caldognetto, T.; Buso, S. Flexible control of interlinking converters for DC microgrids coupled to smart AC power systems. *IEEE Trans. Ind. Electron.* **2019**, *66*, 3477–3485.
35. Wang, J.; Jin, C.; Wang, P. A uniform control strategy for the inter-linking converter in hierarchical controlled hybrid AC/DC microgrids. *IEEE Trans. Ind. Electron.* **2018**, *65*, 6188–6197.
36. Li, X.; Li, Y.; Guo, Z.; Hong, C.; Zhang, Y.; Wang, C. A unified control for the DC-AC interlinking converters in hybrid AC/DC microgrids. *IEEE Trans. Smart Grid* **2018**, *9*, 6540–6553.
37. Yang, P.; Xia, Y.; Yu, M.; Wei, W.; Peng, Y. A decentralized coordination control method for parallel bidirectional power converters in a hybrid AC-DC microgrid. *IEEE Trans. Ind. Electron.* **2018**, *65*, 6217–6228.
38. Xia, Y.; Peng, Y.; Yang, P.; Wei, W. Distributed coordination control for multiple bidirectional power converters in a hybrid AC/DC microgrid. *IEEE Trans. Power Electron.* **2017**, *32*, 4949–4959.
39. Heier, S. *Grid Integration of Wind Energy Conversion Systems*; Wiley: Hoboken, NJ, USA, 2006.
40. Valverde, L.; Bordons, C.; Rosa, F. Integration of Fuel Cell Technologies in Renewable -Energy-Based Microgrids Optimizing Operational Costs and Durability. *IEEE Trans. Ind. Appl.* **2016**, *63*, 167–177.
41. Ucar, M.; Ozdemir, E. Control of a 3-phase 4-leg active power filter under non-ideal mains voltage condition. *Electr. Power Syst. Res.* **2008**, *78*, 58–73.
42. Villanueva-Rosario, J.A.; Santos-Garcia, F.; Aybar-Mejia, M.E.; Mendoza-Araya, P.; Molina-García, A. Coordinated ancillary services, market participation and communication of multi-microgrids: A review. *Appl. Energy* **2022**, *308*, 118332.